Boundary-Layer Meteorology (2025) 191:3
https://doi.org/10.1007/s10546-024-00893-7

RESEARCH ARTICLE

Impact of Surface Heterogeneity Induced Secondary Circulations on the Atmospheric Boundary Layer

Sreenath Paleri[1,2,3] · Luise Wanner[4,5] · Matthias Sühring[6,7] · Ankur R. Desai[1] · Matthias Mauder[4,5] · Stefan Metzger[1,8,9]

Received: 12 October 2023 / Accepted: 10 December 2024

Abstract

We investigate how effective surface length scales (L_{eff}) and atmospheric boundary layer stability modulate surface-induced secondary circulations over a realistic heterogeneous surface. The evolution of the circulations and their impact on surface-atmosphere fluxes are studied using coupled large eddy simulations of the CHEESEHEAD19 field campaign. The heterogeneity-induced circulations were diagnosed using time and ensemble averaging of the atmospheric fields. Simulations were performed for summer (August) and autumn (September) Intensive Observation Periods of the field campaign, characterised differently in terms of normalised surface length scales and ABL stability. Quasi-stationary and persistent circulations were diagnosed in the daytime ABL that span the entire mixed layer height (z_i). Their variation in time and space are presented. Homogeneous control runs were also performed to compare and contrast spatial organisation and validate the time-ensemble averaging operation. In the convective boundary layers simulated during the summer time simulations, wavelengths that scale as the effective surface heterogeneity length scales contribute the most to the heterogeneity-induced transport. Contributions from surface-induced circulations were lower in the simulated near-neutral BL for the autumn simulations. We find that both L_{eff}/z_i and ABL static stability control the relative contribution of surface-induced circulations to the area averaged vertical transport. This scale analysis supports prior work over the study domain on scaling tower measured fluxes by including low frequency contributions. We

---

✉ Sreenath Paleri
paleri@wisc.edu

[1] Department of Atmospheric and Oceanic Sciences, University of Wisconsin-Madison, Madison, WI, USA

[2] Present Address: Cooperative Institute for Severe and High-Impact Weather Research and Operations, University of Oklahoma, Norman, OK, USA

[3] Present Address: Atmospheric Turbulence and Diffusion Division, NOAA/Air Resources Laboratory, Oak Ridge, TN, USA

[4] Institute of Hydrology and Meteorology, TUD Dresden Technical University, Dresden, Germany

[5] Institute of Meteorology and Climate Research - Atmospheric Environmental Research, Karlsruhe Institute of Technology, Garmisch-Partenkirchen, Germany

[6] Institute of Meteorology and Climatology, Leibniz University Hannover, Hannover, Germany

[7] Pecanode GmbH, Goslar, Germany

[8] AtmoFacts, Longmont, CO, USA

[9] CarbonDew, Longmont, CO, USA

believe that the conceptual framework presented here can be extended to include the effects of sub-grid land surface heterogeneity in numerical weather prediction and climate models and also to further explore scale-aware scaling methodologies for near surface-atmosphere exchanges.

Keywords Coupled large eddy simulations · Diurnal simulations · Land surface heterogeneity · CHEESEHEAD19 · Energy balance · Dispersive fluxes

1 Introduction

The continuous exchange of mass, momentum and energy between earth's surface and atmosphere mediated by the atmospheric boundary layer (ABL) has a significant influence on Earth's weather and climate processes (Betts et al. 1996; Pielke et al. 1998). Turbulence is the primary transport process in the atmospheric boundary layer and drives the primary flow. Observations (Lemone 1973, 1976; Weckwerth et al. 1997, 1999; Drobinski et al. 1998; Eder et al. 2015; Träumner et al. 2015) and numerical simulations (Deardorff 1972; Moeng and Sullivan 1994; Avissar and Schmidt 1998; Khanna and Brasseur 1998) have reported coherent secondary circulations in the turbulent ABL. In forced convective boundary layers, with strong mean winds, these structures organise as horizontal convective rolls (Lemone 1973; Etling and Brown 1993) and in free convective boundary layers, when the mean wind shear is weaker and surface fluxes stronger, they organise into open convective cells, akin to the cellular structures in turbulent Rayleigh-Bénard convection (Atkinson and Wu Zhang 1996; Salesky et al. 2017). In the ABL over homogeneous surfaces, these secondary circulations can arise from randomly generated slow-moving turbulent organised structures (Kanda et al. 2004; Inagaki et al. 2006). With heterogeneous surface forcings, horizontal gradients of surface properties, such as patches of different temperature or forest and lake edges, can induce quasi-stationary sub-mesoscale circulations (Blanford et al. 1991; Hadfield et al. 1991; Letzel and Raasch 2003; Inagaki et al. 2006; Maronga and Raasch 2013; Anderson et al. 2015; Kenny et al. 2017; Fogarty and Bou-Zeid 2023). With these conditions, one cannot assume that the ABL flow is horizontally homogeneous. This can complicate classical theoretical frameworks and modelling approaches for surface-atmosphere transport such as the Monin-Obukhov Similarity Theory (MOST) frameworks. These quasi-stationary circulations can hence bias fixed-point turbulent flux estimates from flux measurement towers (Kanda et al. 2004; Steinfeld et al. 2007; Prabha et al. 2007; De Roo and Mauder 2018) if they are not carried past the towers by the mean wind and also modulate surface layer turbulent transport (Salesky and Anderson 2018; Margairaz et al. 2020; Zhou et al. 2023).

Most simulation studies investigating the role of secondary circulations in the ABL have involved idealised surface heterogeneities (Inagaki et al. 2006; Huang et al. 2009; Sühring et al. 2014; Margairaz et al. 2020; Gryschka et al. 2023). Initial studies started out with using prescribed 1D, stripe like or sinusoidal heterogeneities (Hadfield et al. 1992; Avissar and Schmidt 1998) and later studies exploring the effects of 2D prescribed surface fluxes (Shen and Leclerc 1995; Raasch and Harbusch 2001; Liu et al. 2011). Subsequently, LESs with coupled land surface models (LSM) were used to study the coupling between surface heterogeneities and vertical structure of the Convective Boundary Layer (CBL) (Albertson et al. 2001; Kustas and Albertson 2003; Courault et al. 2007).

Patton et al. (2005) studied the effects of surface heterogeneity length scales relative to the boundary layer height using idealised stripe-like heterogeneities in a coupled LES - LSM without any imposed mean wind. They found the strongest surface-heterogeneity induced circulations for heterogeneity scales ranging from 4 to 9 times the ABL height (z_i). Courault et al. (2007) reported that smaller scale heterogeneities (1.25 to 5 km) with horizontal wind speeds of 3–4 m s^{-1} can generate secondary circulations along surface thermal and soil moisture gradients. Prabha et al. (2007) studied the secondary circulation characteristics over irregular surface heterogeneities with prescribed surface fluxes derived from remote sensing and eddy covariance (EC) measurements, 2 m s^{-1} imposed winds with varying directions, and periodic boundary conditions. They reported that the orientation of surface heterogeneities with respect to geostrophic wind, along with the horizontal scale and amplitude of surface heat flux gradients strongly influence the strength, location and organisation of secondary circulations.

Maronga and Raasch (2013) (hereafter referred to as MR13) investigated the CBL response to prescribed heterogeneous surface heat fluxes that represented the observed near-surface fluxes during the LIFASS-2003 field campaign. Using time and ensemble averaging, they diagnosed surface heterogeneity-induced quasi-stationary secondary circulations separating them out from the random turbulent organised structure signals. The heterogeneity-induced structures in their case studies were roll-like or local structures based on the imposed geostrophic wind speed and spanned the entire CBL height. However, they did not investigate the role of the length scales of surface heterogeneities in modulating the organization of and transport due to secondary circulations. They did a correlation analysis of upstream fetch of the surface flux and surface-induced vertical wind. But the surface length scales were not quantified. Consequently,their study also did not look into how changing ABL static stability could alter the role of surface heterogeneity length scales over a realistic domain.

Secondary circulations in the ABL can contribute towards area averaged vertical transport through the spatial covariance of time-mean fields, that are referred to as dispersive fluxes (Wilson and Shaw 1977; Raupach and Shaw 1982). Investigating the dispersive flux contributions over idealised surface heterogeneities using LESs, Margairaz et al. (2020) reported that mean winds over 4 ms^{-1} tend to smear out the influences of the underlying surface heterogeneities. They investigated the role of surface thermal heterogeneities by prescribing patches of different length scales.

MR13 diagnosed roll-like circulations in the ABL induced by surface heterogeneities for strong background geostrophic wind speeds (wind speeds $\sim$ 3–6 ms^{-1}) as well. Although they had a diurnal variation in their imposed surface heat fluxes, the imposed geostrophic wind forcings were kept constant for their case studies, with periodic boundary conditions. This limited the capability of their setup to explore the flux contributions from surface heterogeneity-induced circulations with diurnal changes in ABL static stability. Moreover, their study used prescribed surface fluxes, thereby decoupling the land surface from the atmospheric effects. The idealised LES study of Wanner et al. (2022b) reported that, a coupled LES-LSM combined with a Plant Canopy Model (PCM) can have stronger secondary circulations, and significantly larger transport due to those circulations. We build on their idealised setup to simulate the land-atmosphere coupling over a more realistic study domain with multiple scales of surface heterogeneities.

The strength and vertical extent of ABL flow field modifications by surface heterogeneities can depend on the relative magnitude of surface length scales. In the real world, surface variability can be composed of a range of scales superimposed over each other. To study the boundary layer response to irregular and multi-scale surface forcings one can start with the assumption that a heterogeneous land surface can be conceptualised as a mosaic of multiple surface patches. Here, the properties of individual surface elements can be assumed to be statistically uniform within the patches such that the surface can be thought of as a collection of patches with bulk surface properties, whose intra-patch variance is more significant than the inter-patch variances (van Heerwaarden et al. 2014; Mahrt 2000; Bou-Zeid et al. 2020).

Then, for a given study domain of interest, one can define an effective surface length scale (L_{eff}), which would be a property of the spatial arrangement of surface patches, that can encode information about the dominant spatial scale of surface flux variability. To get a first order understanding of the coupled, multi-scale, surface-atmosphere transport, such a length scale could indicate the dominant wavelength that corresponds to a majority of surface flux variability, the dominant spatial scale at which the land surface is forcing the ABL.

For relatively smaller surface heterogeneity length scales, when $L_{eff} < z_i$, that are referred to as micro-scale heterogeneities (Mahrt 2000; Bou-Zeid et al. 2020), the surface effects can get blended above some height in the boundary layer through turbulent mixing. When the surface heterogeneity scales are larger than z_i they can induce circulations that can affect the entire boundary layer (Shen and Leclerc 1995; Albertson et al. 2001; Raasch and Harbusch 2001; Sühring and Raasch 2013).

Here, we start from this understanding to investigate the ABL spatial organisation over realistic, unstructured, surface heterogeneities and the role of spatially persistent secondary circulations in area-averaged ABL transport. Prior studies mentioned above have largely investigated secondary circulations induced by idealised surface heterogeneities. Previous studies with realistic surface forcings, like MR13 and Albertson et al. (2001) used prescribed surface forcings, with cyclical boundary conditions and constant geostrophic winds. Although they found correlations between surface and atmospheric fields, the effective surface length scales were not quantified and this prevented a direct comparison with surface-induced atmospheric length scales. Furthermore, they did not investigate the contribution from surface-induced circulations to dispersive fluxes, as mediated by the length scales of surface heterogeneities.

In this study, we quantify the dispersive flux contributions (and the share of surface heterogeneity-induced dispersive fluxes) for a more realistic, heterogeneous surface. We also present a framework to quantify effective surface length scales over unstructured heterogeneities, that can be generalised to investigate spatial organisation of ABL flow. We build on the coupled, realistic large eddy simulation framework presented and validated in Paleri et al. (2023), where we parameterised, ran and evaluated an ensemble suite of LESs over the CHEESEHEAD19 field experiment domain for the diurnal ABL. CHEESEHEAD19 was a field campaign designed to intensively sample and scale land surface properties and the ABL response to them. The campaign was conducted in a heterogeneous mid-latitude forested domain in Northern Wisconsin, USA as the study domain transitioned from late summer to early autumn (Butterworth et al. 2021).

We hypothesise that over irregular, unstructured surface heterogeneities, one can define cross-wind surface length scales that impose themselves on the ABL flow and modulate the transport due to surface-induced circulations to the area averaged flux transport in the ABL via the dispersive fluxes they induce. We seek to answer the following research questions: How do the length scales of irregular, unstructured heterogeneities modulate the spatial organisation of secondary circulations in the heterogeneously heated ABL? And, in turn, how is the contribution from surface-induced secondary circulations to the area averaged mixed layer transport controlled by ABL static stability and surface length scales? We quantify the non-dimensional length scales of the unstructured, heterogeneous land surface as L_{eff}/z_i, where L_{eff} is calculated from Fourier spectra of the characteristic surface temperature and moisture fields (θ_*, q_*).

Section 2 presents a synopsis of the LES framework, calculation of dispersive fluxes and their surface-induced component (the time-ensemble averaging routines), calculations for effective surface length scales and ABL flow parameters. Section 3 presents an analysis of the simulated ABL temporal evolution and spatial organisation, and a scale analysis of the diagnosed surface-induced fields 3D fields. Section 4 answers our proposed research questions based on our simulation data and discusses some additional considerations elucidated by this dataset. Section 4.5 provides a brief summary of the manuscript and gives an outlook for future studies.

2 Methods

2.1 Large Eddy Simulations Set Up and Case Studies

We used the PArallelized LES Model (PALM) (Maronga et al. 2020) revision number 21.10-rc.2 for the numerical simulations. PALM solves the non-hydrostatic, filtered, incompressible Navier–Stokes equations in Boussinesq-approximated form on an Arakawa staggered C-grid (Harlow and Welch 1965; Arakawa and Lamb 1977). Prognostic equations are solved for the velocity components u, v, w, the potential temperature θ, water vapour mixing ratio q, a passive scalar s and the subgrid-scale turbulent kinetic energy (SGS-TKE) e. The sub-grid scale terms are parameterised using the 1.5 order turbulent kinetic energy scheme of Deardorff (1980) modified by Moeng and Wyngaard (1988) and Saiki et al. (2000). The advection terms were discretised using a fifth-order scheme (Wicker and Skamarock 2002), and a third-order Runge–Kutta scheme by Williamson (1980) was used for the time integration.

Paleri et al. (2023) gives a detailed description of the PALM model setup used for this study and validation of the case study days against the field campaign measurements. We give a brief description of the model setup and configuration below.

To realistically simulate the surface atmospheric interactions over the heterogeneous CHEESEHEAD19 domain the LES were run with a coupled Land Surface Model (LSM) combined with a Plant Canopy Model (PCM), for the surface boundary conditions. The LSM setup was informed by data from the Wiscland 2.0 digital database (Wisconsin Department of Natural Resources, Fig. 1) which is a land cover map of the entire state of Wisconsin with a resolution of 30 m and providing multiple levels of detail. The leaf-area density (LAD) profiles for the PCM are based on field observations at 9 forested sites within the CHEESEHEAD19 study area. The observed profiles were classified as broadleaf, needle leaf and mixed forests. The grouped LAD profiles were then averaged and finally re-sampled to the PALM grid spacing.

We performed diurnal simulations for two consecutive days during the summer and autumn Intensive Observation Periods (IOP) of the field experiment. August 22 and 23 were chosen for the summer IOP and September 24 and 25 for the autumn IOP. The experimental conditions were more free convective during the August IOP days than during the September IOP days, when they were more wind-shear driven and forced convective (Paleri et al. 2022). So choosing these two test cases lets us compare and contrast the secondary circulations between two different dynamic stability regimes.

To simulate the diurnal variations during the field experiment with evolving synoptic conditions over a heterogeneous study domain, non-stationary lateral and top boundary conditions were prescribed for the simulations using an offline-nesting approach (Kadasch et al. 2021). Large scale forcing data for the boundary conditions were prepared using the National Centers for Environmental Prediction - High Resolution Rapid Refresh (NCEP-HRRRv4) version of the Weather Research and Forecasting - Advanced Research WRF (WRF-ARW)

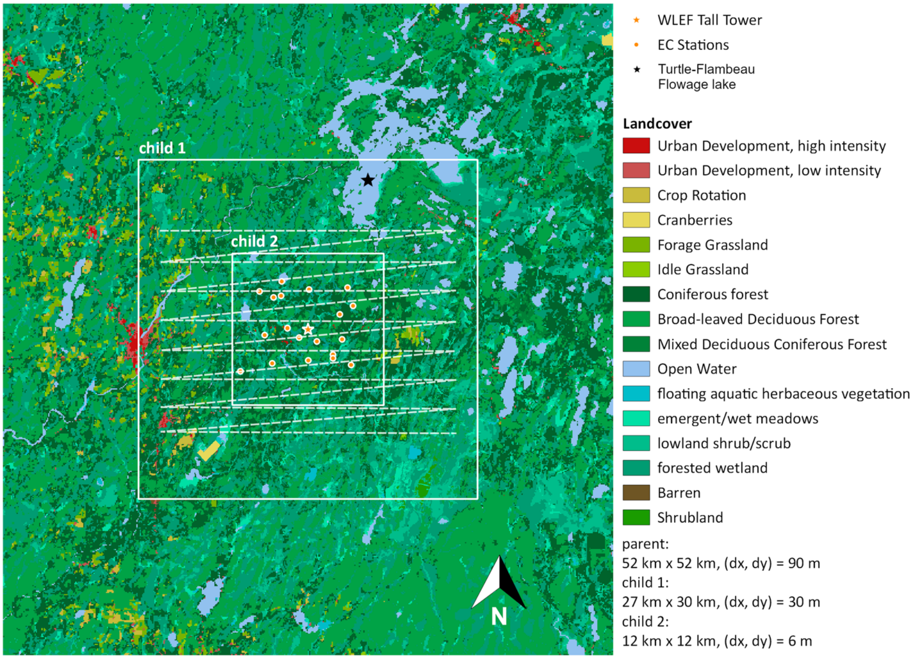

Fig. 1 Land surface class distribution within the Parent model domain. Child01 model is shown as a 27 × 30 km^2 box outlined in white. Child02 model domain is shown as a white outlined 12 × 12 km^2 box within Child01. The upward pointing arrow to the bottom right indicates geographic north. The orange dots within Child02 denote the CHEESEHEAD19 tower locations. The orange star indicates the location of the US-PFa tall tower. The black star indicates the Turtle-Flambeau Flowage lake to the north in the model domains. The dotted white line over Child02 is a representative virtual flight pattern which was set up in Child01

model (Benjamin et al. 2016) with a native horizontal resolution of 3 km. 3D isobaric data were extracted from the University of Utah HRRR archive (Blaylock et al. 2017) and interpolated to the PALM model grid.

Three nested model domains were set up. The Parent domain had a horizontal resolution of 90 m and was centred around the Department Of Energy Ameriflux regional tall tower (US-PFa, 45.9459° N, −90.2723° W, Desai et al. (2022)) covering a 48.6 × 52 km^2 region, to guarantee that turbulence is fully developed in the study area of interest. Since the large-scale forcing data does not have resolved turbulence, adjustment zones are needed to allow for turbulence development at the inflow boundary so that realistic turbulence is simulated within the domain of interest. One-way nesting was deployed between the three nested domains, with the outermost Parent model receiving input from the larger-scale model and two children (Child01 and Child02, Fig. 1) recursively nested within the outermost Parent model. In this setup, only the outermost Parent model requires the initialisation and boundary data from the larger-scale model. The maximum model timestep for all models was kept fixed at 0.6 s.

In this study, we focus on the simulated data from the Child01 model domain, covering a 27 × 30 km^2 region horizontally and extending 2.49 km vertically for the August simulations and 1.8 km vertically for the September simulations. The numerical grid spacing was set at 30 m horizontally and 12 m vertically. The daytime data during 23 August and 24 September simulations are analysed for this study, when all of the ABL was fully resolved within the Child01 model.

2.1.1 Homogeneous Control Runs

To investigate the role of surface heterogeneities compared to homogeneous surface forcings, control runs with prescribed homogeneous surface forcings were set up. The lateral and model top boundary conditions were kept the same. Simulations of the Parent and Child01 models were done.

Surface heat and moisture flux values to be prescribed for the Parent and Child01 homogeneous models were picked from the simulated, horizontally domain-averaged vertical fluxes in the heterogeneous runs. Time series of the domain mean fluxes (resolved + sub-grid contributions) above the canopy top at 36 m grid level were prescribed for the homogeneous runs. A constant aerodynamic roughness of 3 m was prescribed throughout the model domain. Maximum canopy height for the heterogeneous cases was 30 m, so roughness height of 3 m corresponds to 0.1 times this as a first order approximation for an idealised homogeneous canopy.

2.2 Data Analysis

To be able to answer our Research Question 1, on the role of the length scales of surface heterogeneities, we start with calculating the near-surface characteristic temperature and moisture fields, θ_* and q_*, to quantify the length scales of surface heterogeneities. θ_* and q_* were calculated from the near-surface kinematic heat and moisture flux fields using the domain-mean, near-surface u_* values like so:

$$\overline{\theta_*} = \frac{\overline{w'\theta_0'}}{\langle u_* \rangle}, \ \overline{q_*} = \frac{\overline{w'q_0'}}{\langle u_* \rangle}, \tag{1}$$

where $\overline{w'\theta_0'}$ and $\overline{w'q_0'}$ are the near-surface, above canopy kinematic heat and moisture fluxes. The near-surface flux data was calculated as the sum of the LSM flux output and the vertically integrated canopy heat fluxes from the PCM. For the homogeneous control runs, imposed values of surface fluxes, $\overline{w'\theta_0'}$ and $\overline{w'q_0'}$, were used (which match the Child01 model flux values at 36 m).

Effective horizontal heterogeneity length scales (L_{eff}) were calculated in the along-wind and cross-wind directions for the study domain from the Fourier spectra of θ_* and q_* transects. Since the location of the spectral maximum can be noisy, for each transect, the spatial wavelength contributing to 2/3 of the variance from the smallest scale up was chosen as a critical wavelength (de Roode et al. 2004) to represent the dominant surface heterogeneity scale. The effective along-wind (L_x) and cross-wind length (L_y) scales were calculated as the average of the critical wavelengths for all the transects for both the θ_* ($L_{\theta x}$,$L_{\theta y}$) and q_* (L_{qx},L_{qy}) fields.

To understand how spectral energy is partitioned between different scales of motion in the resolved flow field at different heights we use spectrograms. They have been used to study the scale decomposition of LES simulated resolved scale flows over idealised surface heterogeneities (Brunsell et al. 2011; Margairaz et al. 2020). At each model vertical level, the 2D horizontal data was rotated in to align with the mean ABL wind direction. 1D Fourier spectra and/or cospectra were calculated for all the fields analysed in both cross-wind and along-wind directions, up to the domain mean z_i. The spectra were then normalised by the total power at each vertical level, to pick out the dominant scales at each height.

The 2D ABL height field was calculated as the local maximum of $d\theta(x, y)/dz$ following Sullivan et al. (1998). The domain mean boundary layer height, $\langle z_i \rangle$, was then calculated from these 2D fields. We use the z_i computed by this local-gradient method over the heterogeneous domain for scaling purposes, as suggested by MR13.

The ABL stability parameter, $-z_i/L$, was then calculated from the domain means of the 30-minute averaged data, with $L = -\frac{\langle\overline{\theta_v}\rangle\langle u_*\rangle^3}{kg(\langle\overline{w'\theta'_{v0}}\rangle)}$ being the Obukhov length calculated above the canopy at 36 m. Here, $\langle\overline{\theta_v}\rangle$ is the domain and 30-minute mean virtual potential temperature, $\langle u_*\rangle$ is the surface layer friction velocity calculated at the same height, k is the von Kármán constant taken to be 0.4, $g = 9.8\ \mathrm{ms}^{-2}$ the acceleration due to gravity and $\langle\overline{w'\theta'_{v0}}\rangle$ the near-surface buoyancy flux at the same height.

Spatial variances presented in this manuscript are horizontal spatial variances calculated with respect to the spatial mean at the respective vertical grid level. For instance, for the time mean 4D LES data for vertical wind, it was calculated as:

$$\sigma^2_{\overline{w}(z,t)} = \langle(\overline{w}(x, y, z, t) - \langle\overline{w}\rangle(z, t))^2\rangle. \tag{2}$$

Here, the term in parenthesis $(\overline{w}(x, y, z, t) - \langle\overline{w}\rangle(z, t)))$ is the spatial deviation at every horizontal grid point for all vertical grid points, for the corresponding 30-minute timesteps.

2.3 Dispersive Fluxes From Secondary Circulations

Spatially averaging the time-averaged equations of motion will give rise to sub-filter (considering the averaging operators as filters) scale terms, that have been referred to as dispersive covariances (Wilson and Shaw 1977; Raupach and Shaw 1982). Here we present a brief overview of their theoretical basis, physical interpretation and how we calculate them for our analysis of the area averaged mixed layer transport. Then we build upon this framework, using time-ensemble averaging to filter out the surface-induced contribution to the dispersive fluxes to answer our Research Question 2.

Suppose $\bar{.}$ represents the time averaging operator and $'$ denotes the instantaneous fluctuation from the same, the instantaneous 3D velocity field, u_i, can be written as their sum, following a traditional Reynolds decomposition: $u_i = \overline{u_i} + u'_i$. For a horizontal average across a chosen spatial domain, $\overline{u_i} = \langle\overline{u_i}\rangle + \overline{u_i}''$, where $\langle.\rangle$ denotes the spatial averaging operator and $''$ denotes the local spatial deviation from the domain mean. Hence, a double averaging procedure of the equations of motion, involving first a temporal averaging and then a spatial averaging, would yield covariance terms such as $\langle\overline{u_i}''\overline{u_j}''\rangle$ and $\langle\overline{u'_i u'_j}\rangle$, such that the total spatial covariance within the control volume so chosen is given by their sum (Raupach and Shaw 1982).

The double averaging procedure can be extended for the scalar conservation equations, for an arbitrary scalar Φ, in the vertical direction:

$$\langle\overline{w''\Phi''}\rangle(z) = \langle\overline{w}''\overline{\Phi}''\rangle(z) + \langle\overline{w'\Phi'}\rangle(z). \tag{3}$$

Here, the first term on the right is termed the dispersive flux of the scalar (Margairaz et al. 2020; Wanner et al. 2024) and the second term is the domain-mean of the local turbulent flux, calculated as the Reynolds averaged temporal-covariance. Hence, dispersive fluxes are the spatial covariances between the time mean velocity and scalar fields. Over homogeneous surfaces, the coherent structures are turbulent organised structures. They contribute to the domain mean total spatial covariance through the dispersive fluxes. For flow over heterogeneous surfaces, surface heterogeneities can cause circulations that are persistent in space (standing cells, or internal boundary layers) or they could make the non-persistent, random turbulent organised structures pinned to a location. In this manuscript we investigate the latter, and look into the cases where surface heterogeneities cause coherent turbulent structures to be persistent in space. Their effects, if any and in either, should hence be reflected in the dispersive fluxes for the study domain, or how they are different from the representative homogeneous case study.

The domain mean dispersive flux profiles at all vertical grid point was calculated as the spatial covariance between 30-minute averaged vertical velocity and the 30-minute averaged variable of interest, $\Phi(x, y, z)$ like so:

$$\langle \overline{w}''\overline{\Phi}'' \rangle(z) = \frac{1}{nx \times ny} \sum_{1}^{nx} \sum_{1}^{ny} (\overline{w}(x, y, z) - \langle \overline{w} \rangle(z))(\overline{\Phi}(x, y, z) - \langle \overline{\Phi} \rangle(z)). \tag{4}$$

2.3.1 Surface Induced Dispersive Fluxes

For idealised and regular surface heterogeneities, signals of surface induced circulations can be isolated from the primary turbulent flow field by spatially averaging the temporal means over similar surface patterns, like a phase averaging operation (Raasch and Harbusch 2001; Patton et al. 2005). For irregular surface heterogeneities with no repeating surface patches or axis of similarity to subset the data by, one can employ temporal and ensemble averaging to filter out signals of random turbulent convection (Maronga and Raasch 2013). Here, ensemble averaging is akin to statistically prolonging the time averaging through multiple realisations of the flow field that are stitched together and averaged in turn. In that sense, if ensemble means remove the contributions from random, turbulent motions, then the spatial covariance between time-ensemble mean fields would be due to the persistent circulations and scalar fields induced by surface heterogeneities.

We use 30-minute time means and ensemble simulations to diagnose surface induced contributions to surface-atmosphere fluxes over the CHEESEHEAD19 study domain.

Any 4D quantity $\Phi(x, y, z, t)$ over a heterogeneous domain, can be decomposed to a surface heterogeneity induced and smaller scale turbulent components as (Maronga and Raasch 2013; Patton et al. 2005):

$$\Phi(x, y, z, t) = \langle \Phi \rangle(z, t) + \Phi_{hi}(x, y, z, t) + \Phi_s(x, y, z, t), \tag{5}$$

where $\langle . \rangle$ denote horizontal domain spatial averages, the subscript hi denotes the surface heterogeneity induced part and subscript s denotes the small scale turbulent part. Time and ensemble averaging Eq. 5:

$$\Phi_{hi}(x, y, z, t) = \widetilde{\overline{\Phi(x, y, z, t)}} - \widetilde{\overline{\langle \Phi \rangle(z, t)}}, \tag{6}$$

where the $\widetilde{.}$ denote ensemble averages and we assume that $\widetilde{\overline{\Phi_s(x, y, z, t)}} = 0$. Horizontal averaging of Eq. 6 gives $\langle \Phi_{hi}(x, y, z, t) \rangle = 0$, so that $\Phi_{hi}(x, y, z, t)$ is the surface heterogeneity induced spatial variation from the domain mean state for the averaging time interval. That means,

$$\Phi_{hi}(x, y, z, t) = \widetilde{\overline{\Phi(x, y, z, t)}}''. \tag{7}$$

Equipped with such a scale separation, we can decompose the domain mean total vertical flux of $\Phi(x, y, z, t)$ as (Eq. 9 in Chen and Avissar (1994), Eq. 16 in MR13):

$$\langle \overline{w\Phi} \rangle(z) = \overline{\langle w \rangle \langle \Phi \rangle}(z) + \langle w_{hi}\Phi_{hi} \rangle(z) + \langle \overline{w_s\Phi_s} \rangle(z). \tag{8}$$

The first term on the r.h.s of Eq. 8 is the mesoscale flux associated with the imposed large scale flow, the second term is the domain mean mesoscale flux induced by land surface heterogeneities and the third term is the simulated turbulent scale fluxes. Since we are not interested in the fluxes due to the imposed large scale forcings, their contributions as per term 1 was removed while writing out half hourly averaged data outputs. Hence, for the ensemble mean fields, if contributions from the first term on the RHS of Eq. 8 are removed, we are left with:

$$\widetilde{\langle \overline{w\Phi} \rangle}(z) = \langle \widetilde{\overline{w}}''\widetilde{\overline{\Phi}}'' \rangle(z) + \widetilde{\langle \overline{w'\Phi'} \rangle}(z), \tag{9}$$

where the first term on the right hand side is the dispersive flux of Φ from the time-ensemble mean field (equivalent to the LHS of Eq. 4), and the second term on the right is the ensemble mean of the spatial average of Reynolds averaged turbulent fluxes.

2.4 Ensemble Realisations

Each ensemble simulation is characterised by unique realisations of the instantaneous turbulent 3D wind fields which are not correlated across the ensemble members. Previous studies using PALM, like MR13 or Sühring et al. (2014) altered the random perturbations imposed onto the horizontal velocity fields, which are used to generate turbulence during the initial model spin up phase. This approach works well with cyclic boundary conditions, however, it fails with non-cyclic boundary conditions as the imposed random perturbations are transported out of the model domain. Therefore, a different approach for random perturbations was followed.

With non-cyclic boundary conditions, to achieve independent turbulent flow realisations in each of the ensemble runs, we altered the scaled random perturbations imposed at the lateral boundaries instead. At the coarse root domain, perturbations calculated according to Xie and Castro (2008) and are imposed onto the lateral boundaries to trigger the development of turbulence from the "laminar" mesoscale forcing data, as described in Kadasch et al. (2021). For each ensemble run we altered the seed in the random number generator, so that for each ensemble run a different set of time-dependent random perturbations was used to calculate scaled perturbations. This ensures a different development of the turbulent flow field in each ensemble run, while the turbulence statistics are invariant across the ensemble runs.

A further source of persistent structures in non-cyclic LES is the mesoscale forcing data. Possible numerical artefacts which may be present in mesoscale model data-sets (especially under convective conditions) enter the LES domain and create persistent role-like structures in the LES that propagate further downstream as described in Mazzaro et al. (2017) or Kadasch et al. (2021). However, for our simulations, we used homogeneous boundary conditions inferred from the HRRR output instead, in order to avoid these persistent structures.

3 Results and Discussion

The spatial variance of the heterogeneity induced vertical velocity, averaged over the ABL height can be used as a metric to check for the convergence of the simulated surface-induced fields, with increasing ensemble members (MR13). Figure 12 shows the ABL averaged $\sigma^2_{w_{hi}}$ calculated with increasing ensemble members. For the August IOP days the profiles slowly converge as the total member number approaches 8. For the September IOP they do not

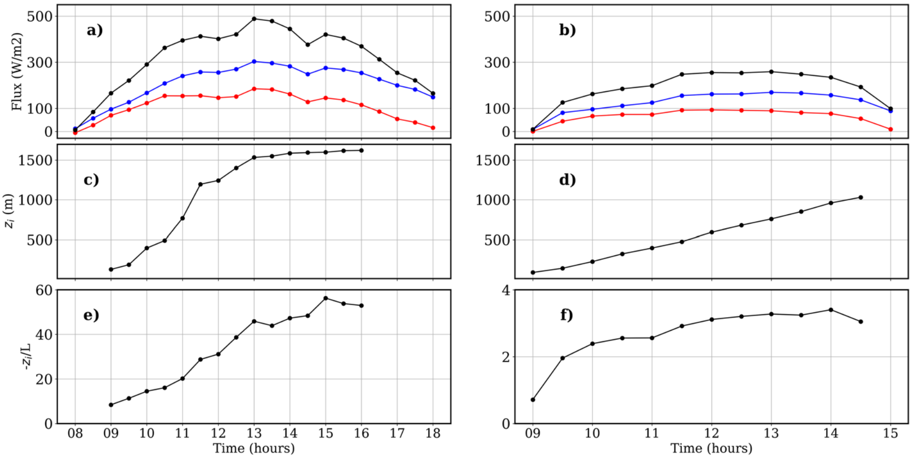

Fig. 2 30-min, domain-mean time series of near-surface (36 m) turbulent fluxes, z_i and ABL static stability (-z_i/L). First column shows calculated values for 23 August (**a**,**c**,**e**) and the second column for 24 September (**b**,**d**,**f**). In the first row, red lines denote H, blue lines LE and black total (H+LE) fluxes

change appreciably after member number 3, indicating a faster convergence, but we simulated 8 members for consistency.

The homogeneous control runs indicated that there were edge effects to the north and east of the Child01 model domain. To remove their effects from our analysis domain we considered a 10×10 km^2 subset of the Child01 model domain for our analysis. The subset domain was chosen to overlap with the core CHEESEHEAD19 field experiment domain. Here, we present our analysis results and ABL variables computed for this 10×10 km^2 domain.

3.1 Atmospheric Boundary Layer Temporal Evolution

Figure 2 presents the 30-minute, domain-mean time series of the simulated near-surface fluxes, ABL height and boundary layer static stability for the heterogeneous 23 August and 24 September simulations. The simulated summertime CBL on 23 August had strong total surface flux forcing, with the total of H and LE ranging from 400 to 500 Wm^{-2} for 1100–1500 CDT (Fig. 2a). The buoyancy driven CBL started growing around 900 CDT and was fully developed by 1300 CDT at 1500 m (Fig. 2b). In early morning, from 0900 to 1100 CDT, as the ABL was growing, the ABL was weakly convective with $z_i/L \in [10, 20]$, due to lower z_i, weaker heat fluxes and stronger mean winds. The boundary layer grew to 1500 m by 1300 CDT and then was stationary till 1630 CDT.

The 24 September simulations had a wind-shear driven, forced convective boundary layer with $z_i/L \sim \mathcal{O}(1)$ and values $\in [1, 3]$. The domain mean boundary layer winds were also stronger, ranging from 4.5 ms^{-1} at 1100 CDT to 7 ms^{-1} at 1330 CDT. The ABL started to grow around 0900 CDT in the morning and grows steadily to 1000 m by 1400 CDT. It remained near neutral throughout the day. The surface buoyancy flux went to near 0 around 1500 CDT and the ABL collapsed very rapidly afterwards, with the near-surface stable boundary layer starting to grow. So, here we present the simulated time series values from 0900 to 1430 CDT.

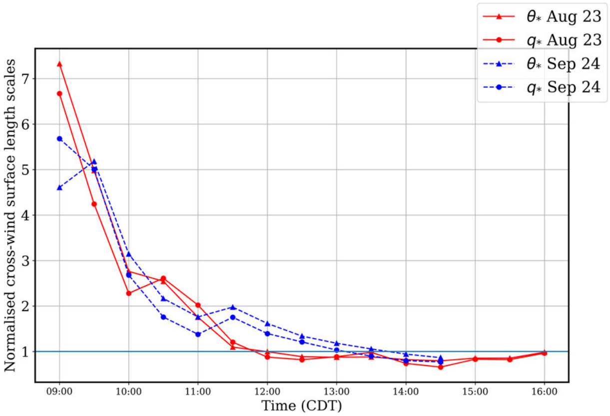

Fig. 3 Cross-wind surface length scales, normalised by z_i (L_y/z_i) for the θ_* (upward triangles) and q_* (filled circles) fields for 23 August (red solid line) and 24 September (blue dashed line) simulations. Horizontal blue line indicates y = 1, when the cross-wind surface heterogeneity length scale = z_i

Normalised cross-wind surface heterogeneity length scales calculated from the θ_* and q_* fields fields are presented in Fig. 3 for the 23 August and 24 September simulations. For Aug. 23^{rd} the relative heterogeneity length scale in the morning $>>$ 1. Later in the day, around 1200 CDT, it becomes $\sim$ 1 and dips below 1 during afternoon (1300–1600 CDT). For September 24^{th} the relative length scale stays greater than 1 for most of the day. It is much greater than 1 in the morning, approaching 2 by 1200 CDT and asymptoting towards 1 in the afternoon.

3.2 Spatial Structure of Diagnosed Heterogeneity Induced Secondary Circulations

The ensemble averaging method as detailed in Sect. 2.3.1 lets us filter out signals of ABL turbulence and diagnose signals of land surface heterogeneity induced coherent ABL structures. Here, we present the ensemble means of the atmospheric θ, q and w fields, with their spatial mean removed, that represents θ_{hi}, q_{hi} and w_{hi}. Horizontal cross-section data from the heterogeneous runs are compared with that from the homogeneous control runs at the same relative model height (relative to z_i) and simulation time to investigate the role of the heterogeneous land surface.

23 August simulations had north-easterly changing to easterly above-canopy winds with a mean magnitude of 2.25 m s^{-1} from 0800 to 1600 CDT. In the morning the ABL is only weakly convective with higher wind speeds than later (Online Resource 2: Fig. 14a).

At 1100 CDT for the 23 August heterogeneous simulations, the persistent spatial fluctuations of the time-ensemble averaged w fields were organised as horizontal convective rolls aligned at an angle to the mean ABL wind (Fig. 4). Along-wind, they extended to almost the whole length of Child01 model $\approx$ 27000 m (Online Resource 4: Fig. 16 shows the organisation in the 30-min mean fields). The vertical wind in homogeneous runs did not have such a strong roll-like organisation. The w_{hi} fields calculated from the homogeneous runs show lesser intensity and much smaller scale roll-like organisation, both near the surface at $0.1z_i$ and in the middle of the ABL (Fig. 4).

There were strong cross-stream gradients of the θ_{hi} and q_{hi} fields calculated from the heterogeneous runs, reflecting the roll-like organisation of the w_{hi} fields. Such strong cross-

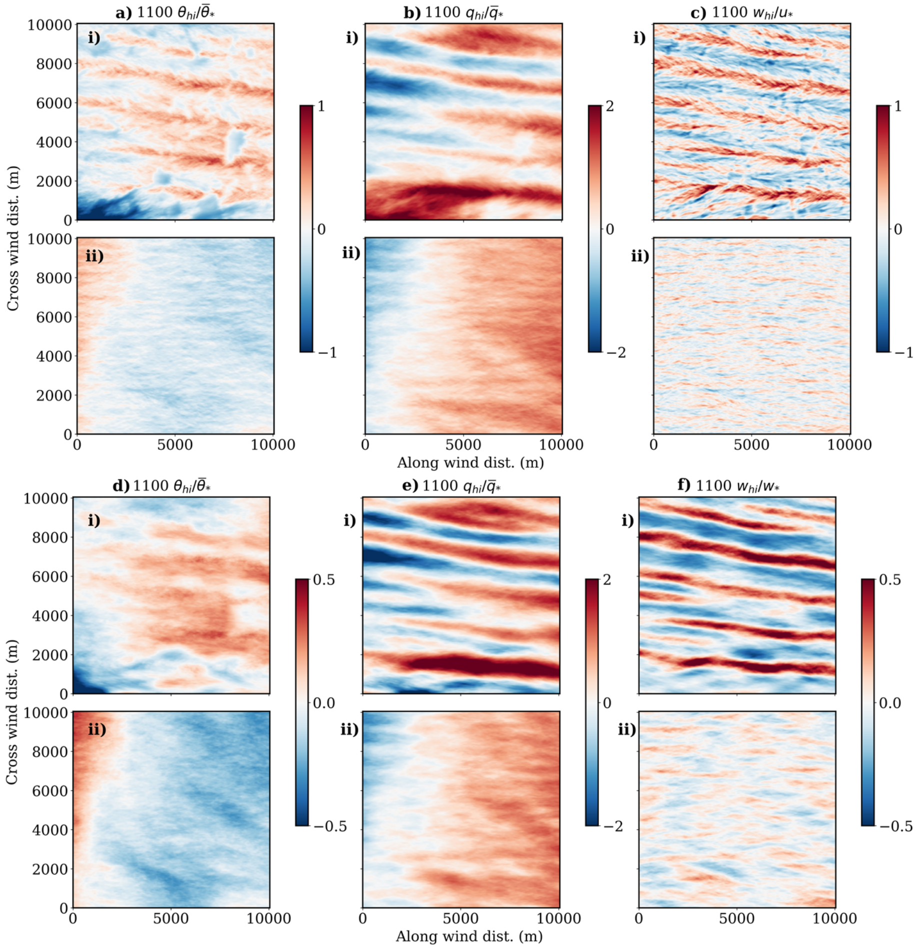

Fig. 4 Normalised, surface induced atmospheric fields, diagnosed from the ensemble means over the 10 × 10 km^2 study domain from the heterogeneous and homogeneous runs at 1100 23rd August. Data presented are rotated to the mean ABL wind direction, such that positive x values indicate distances along the mean wind direction and positive y values the cross-wind direction. Top two rows (**a**–**c**) show horizontal cross-sections at $0.1z_i$ for the heterogeneous runs (i) in the first row and homogeneous runs (ii) in the second row. Bottom two rows (**d**–**f**) show the horizontal cross sections at $0.5z_i$

wind horizontal gradients were absent in ensemble averaged homogeneous fields of θ and q. The homogeneous fields showed a larger-scale, along-wind gradient instead, indicating the stronger influence of larger scale horizontal advection from the imposed large-scale forcing.

The velocity spatial fluctuations in the time-ensemble fields were well correlated to the spatial fluctuations in the scalar fields, implying that the convective rolls in the heterogeneous runs cause local horizontal and vertical advective transport, and contribute strongly toward domain mean dispersive fluxes of θ and q. In other words, the spatial covariance between surface-induced velocities and scalars is higher for the heterogeneous case at 1100 CDT. Imprints of the surface heterogeneity can also be seen in the near surface cross-section plots of θ_{hi} and q_{hi} at $0.1z_i$ (Fig. 4, first row). The moisture fields were more correlated with the

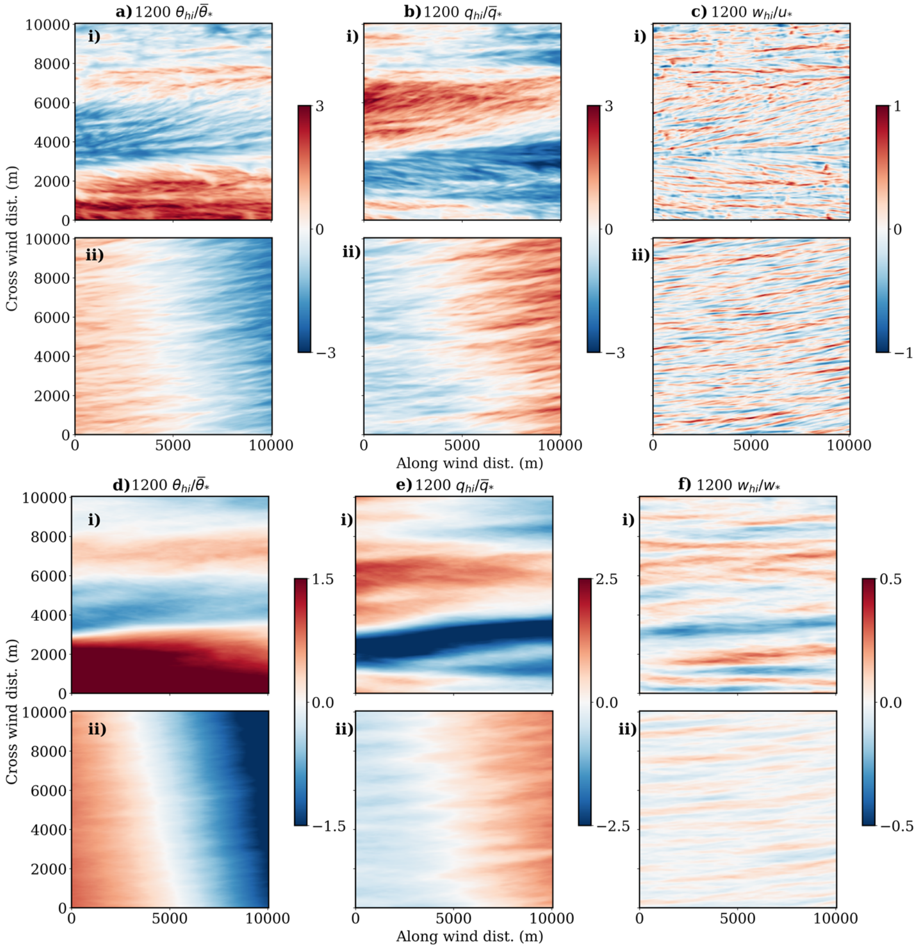

Fig. 5 Same as Fig. 4 but for 1200 24 September, heterogeneous (i) and homogeneous (ii) runs

vertical velocity field than the temperature fields, in both the time-ensemble mean fields and the turbulent large-eddy scales (Online Resource 4, Fig. 16). We see this in wavelet-based, airborne spatial flux measurements from the CHEESEHEAD19 field campaign as well (Paleri et al. 2022; Lin et al. 2024). However, prior studies have reported that the moisture field tends to develop larger structures and lower correlations with the vertical velocity fields (de Roode et al. 2004). We are working on disentangling the surface vs entrainment effects that might be at play over our study domain using both airborne measurements, data from these model runs and additional simulations in a future manuscript.

From 1130 till 1330 CDT, the time-ensemble mean w structures follow the same spatial characteristics as seen at 1100 CDT. They are elongated in the mean ABL wind direction and there is a stronger spatial covariance between the velocity and scalar fields in the heterogeneous cases. Later in the day as the boundary layer grew and became more convective (Fig. 2e), the effective surface length scale to $\langle z_i \rangle$ ratio approached 1 and was lesser than 1 in the afternoon, from 1400 to 1600 CDT (Fig. 3).

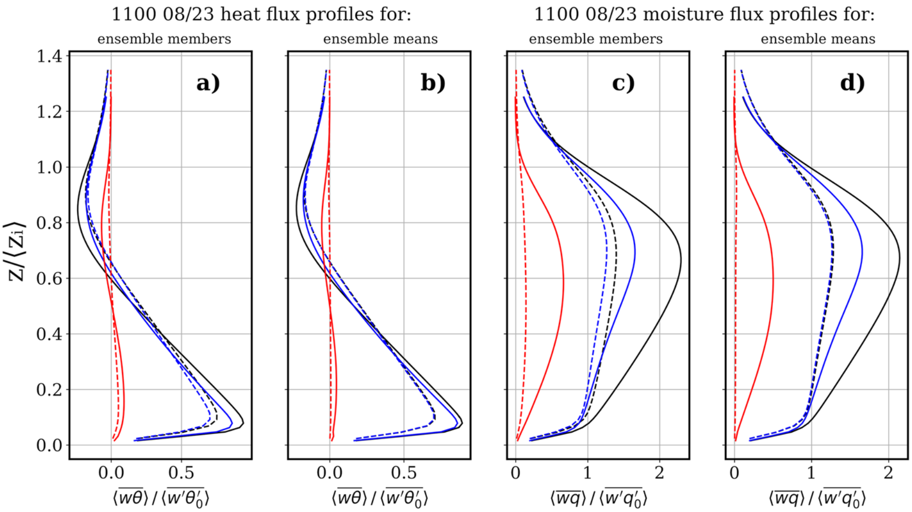

Fig. 6 Domain mean, 30-min averaged turbulent, dispersive and heterogeneity induced vertical kinematic heat (**a**,**b**) and moisture (**c**,**d**) flux profiles. Profiles are shown for the time period ending at 1100 CDT 23 August. Panels **a**, **c** indicate mean values of flux profiles calculated from individual members (representing components of Eq. 3). Panels **b**,**d** are flux profiles calculated from the time-ensemble means (representing components of Eq. 9). Solid lines for heterogeneous runs and dashed lines for homogeneous runs. Blue lines are turbulent fluxes, red lines are dispersive and black lines are total fluxes (sum of red and blue)

Starting from 1400 CDT, there were no qualitative differences between the spatial organisations and strength of θ_{hi}, q_{hi} and w_{hi} between the heterogeneous and homogeneous runs (Online Resource 3: Fig. 15). Using longer time averaging windows, ranging from 60 to 120 min, did not indicate any differences between the homogeneous and heterogeneous fields. Here, we limit our analysis till 1600 CDT, after which the CBL starts to decay with decreasing surface fluxes in the evening and increasing effects of ABL top entrainment. These similarities persisted throughout the afternoon CBL from 1400 to 1600 CDT. This indicated that as the turbulent boundary layer grew and the non-inertial, energy containing turbulent eddies also grew in their spatial scales with it, with surface length scales smaller than the $\langle z_i \rangle$, the surface induced circulations became much weaker in comparison. Resulting in velocity and scalar fields similar to an ABL with homogeneous surface forcings, as elucidated in time-ensemble means that reveal the low-frequency spatial organisation embedded within the primary turbulent flow.

The forced convective ABL in 24 September simulations with stronger near-surface winds showed signals of persistent roll-like heterogeneity induced circulations throughout the duration of the daytime mixed layer. Here we present cross-sections of time-ensemble mean fields at 1200 CDT from the homogeneous and heterogeneous runs, representative of the day time organisation (Fig. 5).

There were differences between the spatial organisation of the atmospheric fields in the heterogeneously forced and homogeneously forced shear-driven ABLs. The heterogeneous simulations showed stronger cross-wind gradients for the normalised θ_{hi} and q_{hi} fields, while the homogeneous values showed a more pronounced along-wind gradient. The organisations were similar to the weakly convective 1100 CDT 23 August runs. However, the θ_{hi} and q_{hi} fields were wider in the cross-wind direction for the 24 September heterogeneous runs than during the morning of the 23 August runs. The cross-wind variations of θ_{hi} and q_{hi} fields show cold-moist and warm-dry along-wind strips. The cold-moist strips are downstream of the Turtle-Flambeau Flowage lake in the north-eastern edge of the model domain (black star in Fig. 1), indicating that the cold-moist air is advected downstream from the lake. This can be seen in the 30-minute mean w, θ, q plots for the entire Child01 model domain presented in the supplement (Online Resource 4, Fig. 16g–l). The w_{hi} field showed much narrower roll-like structures.

The homogeneous control runs also showed roll-like spatial organisation in the diagnosed w_{hi} fields. They were stronger near the surface, indicating the strong near-surface turbulence driven organisation. The amplitude of the normalised w_{hi} fields were weaker at $0.5z_i$ for the homogeneous runs, indicating the stronger blending by atmospheric turbulence over homogeneously forced surfaces. Moreover, the spatial covariances, as can be seen in the relative spatial organisations, between the vertical wind and scalar fields are also weaker in the homogeneous simulations. This is quantified in Sect. 3.3. At 1200 CDT, in the heterogeneous runs, $0.1z_i$ was close to the surface (60 m) and the imprints of localised near-surface thermal and roughness cross-wind gradients can also be seen as local circular maxima in the w_{hi} plot.

Comparing the spatial organisation of θ_{hi} and q_{hi} between the weakly convective morning ABL simulations of 23 August and the near neutral 24 September simulations, a physical picture emerges. In the 23 August morning runs, the stronger (in amplitude) surface flux cross-wind gradients are able to impose themselves on the weaker mean winds aloft, thereby modulating the spatial organisation of the boundary layer scalar and velocity fields. This is clear when comparing the spatial fluctuation fields from time-ensemble means of heterogeneous and homogeneous runs. For the near neutral case, the surface flux amplitudes are weaker and mean ABL winds stronger, that they are able to smear our influences of cross-stream gradients. This has been pointed out in idealised studies Raasch and Harbusch (2001); Patton et al. (2005). There is still a spatial organisation of the boundary layer velocity and scalar fields. The cross-wind length scales in the scalar fields (of spatial fluctuations) are greater than those of the effective surface length scales within the study domain and the velocity fields indicating that they are influenced by larger scale processes, including larger scale heterogeneities upstream and possibly the enhanced larger-scale entrainment fluxes in the shear driven ABL. Their scale composition is investigated further in Sect. 3.4.1.

3.3 Vertical Flux Profiles for the Homogeneously and Heterogeneously Heated ABL

To identify the impact of the heterogeneous surface on vertical fluxes, we compared the domain mean vertical fluxes between the heterogeneous and homogeneous case studies. This helps us to diagnose how strongly the surface modulates spatial covariance between the atmospheric fields. The total spatial fluxes were first decomposed to the turbulent and dispersive components following Eq. 3. Values presented here are the mean values of each ensemble run. From the ensemble mean fields, we calculated the surface-induced dispersive flux contribution, $\langle w_{hi} \Phi_{hi} \rangle$, as well to investigate the total vertical spatial fluxes from the ensemble fields, the first term in the RHS of Eq. 9. Here, we present the flux profiles at 1100 and 1400 CDT for 23 August simulations and 1200 CDT for the 24 September simulations. Flux magnitudes are normalised by above canopy (36 m) fluxes for the heterogeneous runs and the imposed surface fluxes for the homogeneous runs.

In the 23 August simulations at 1100 CDT, in both the homogeneous and heterogeneous runs, most of the total domain-mean fluxes were due to turbulent fluxes (Fig. 6a). The dispersive heat fluxes were very low in the ensemble member simulations and the heterogeneous runs had slightly higher magnitude than the homogeneous runs. In the time-ensemble mean

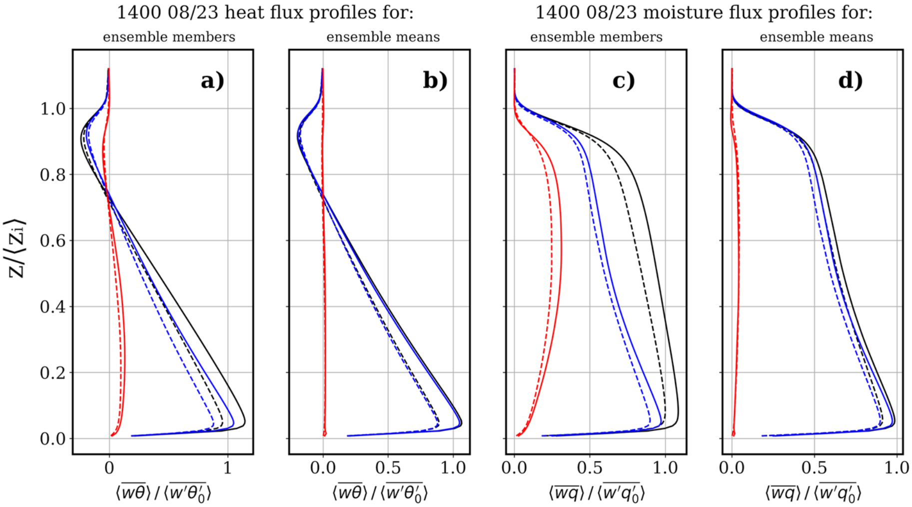

Fig. 7 Same as Fig. 6, but for the time period ending at 1400 CDT 23 August

field for the heterogeneous runs, the entrainment dispersive flux remained the same when compared with the estimate for individual realisations (Fig. 6b) while the time-ensemble mean field in the homogeneous runs had zero contribution from the dispersive heat fluxes. This suggests that the dispersive heat flux contributions are primarily surface-induced. Our simulations indicate surface-induced dispersive fluxes causing entrainment. Sühring and Raasch (2013) and MR13 also reported the effects of heterogeneity reaching till the mixed layer top in their simulations of the LITFASS-2003 field experiment. However, we would like to point out that entrainment effects and their relationship to surface heterogeneities require a more careful analysis before drawing strong conclusions.

The moisture flux profiles at 1100 CDT indicated that the ABL humidity was controlled more by entrainment of drier air from above the mixed layer top than the surface fluxes (Fig. 6c, d). The total entrainment fluxes of water vapour mixing ratio were almost twice as large as the surface fluxes (black lines in Fig. 6c, d).

There were strong contributions from the dispersive fluxes for the heterogeneous runs as compared to the homogeneous runs, whose dispersive flux contributions for the vertical moisture fluxes also remained small. These higher contributions were from the persistent circulations in the time-ensemble mean fields (red solid lines in Fig 6d).

Both the heat and moisture dispersive flux profiles are near zero in the homogeneous runs for the time-ensemble mean flux profiles at 1100 CDT, indicating that the covariance between persistent vertical velocity field and the scalars was negligible. The heterogeneity induced contributions were $\sim 50\%$ of surface fluxes at $0.6z_i$. This result is in line with prior idealised studies Chen and Avissar (1994); Patton et al. (2005) who found that secondary circulations can contribute up to 50–80% of the total flux transport but in contrast to MR13 who reported lower values, 20% for heat and 39% for moisture. There could be a couple of reasons for this difference. First of all, MR13 performed LESs with surface forcings from tower flux data collected during the LITFASS field experiment, characterised by different heterogeneity amplitudes and length scales. Moreover the surface fluxes were prescribed and did not respond to atmospheric fields, thereby missing the surface-atmosphere feedback. Although they did diurnal simulations, they also had periodic boundary conditions, which also could possibly affect the evolution of heterogeneity-induced structures, with a more realistic diurnal evolution of ABL static stability.

At 1400 CDT 23 August, in the fully developed convective boundary layer, the normalised vertical flux profiles in the heterogeneous and homogeneous runs were very similar (Fig. 7). The ensemble averaged fields, for both the homogeneous and heterogeneous runs, indicated that the contributions of surface-induced dispersive fluxes, $\langle w_{hi}\theta_{hi}\rangle$ and $\langle w_{hi}q_{hi}\rangle$, were near zero. This reflects the similarity between the heterogeneous and homogeneous runs in the spatial organisation of the w_{hi},θ_{hi} and q_{hi} fields (Online Resource 3: Fig. 15). Here, when the normalised surface length scales (L_y/z_i) are smaller, the surface induced vertical velocities are also weaker (Fig. 12a), and the ABL secondary circulations are primarily composed of turbulent organised structures.

The dispersive fluxes are slightly larger for the heterogeneous runs, resulting in greater total fluxes in the study domain. This could be due to the higher boundary layer heights in the heterogeneous runs, resulting in the non-inertial ABL scale turbulent eddies having more energy and causing greater transport.

The ABL moisture changes to a surface flux driven regime in the 1400 CDT moisture flux profiles (Fig. 7c). However, the peak in the dispersive moisture flux profile at $0.6z_i$ at 1100 CDT was shifted closer to the ABL top to around $0.8z_i$. This change could be could be due to a couple of reasons, including the weakening inversion strength ($\Delta\theta$, Δq) later in the day as well as a weakening of surface-induced circulations and the related strengthening of non-inertial turbulent structures. Moreover, in the morning boundary layer with stronger surface induced circulations, part of the transport could also be redirected in the along-wind direction, decreasing the entrainment transport (MR13). Signals of this were seen in the vertical profiles of stream-wise moisture flux, where there was a significant peak near the ABL top for the 1100 CDT heterogeneous runs. The entrainment zone behaviour is being analysed in detail to understand the concerned physics and this will be addressed in a follow up study.

For the 23 August simulations, the percentage contribution from dispersive fluxes and their heterogeneity induced component were higher for the moisture flux than the heat flux. LE dominates the surface-atmosphere exchange over H. Both in the smaller turbulent scales and larger landscape scales. Airborne flux measurements over the study domain during the field campaign also reported similar latent and sensible heat flux partitioning across scales Paleri et al. (2022).

The kinematic sensible heat flux profiles for 24 September simulations showed higher mixed layer top entrainment fluxes in the wind-shear driven, forced convective ABL (Fig. 8) compared to the other IOP days. Wind shear across the inversion layer can increase the boundary-layer top entrainment fluxes (Conzemius and Fedorovich 2006; Garcia and Mellado 2014). Moreover, Fig. 8 indicates that there is no significant impact of surface heterogeneity on entrainment on September 24 as the boundary-layer top fluxes for the heterogeneous and homogeneous simulation are almost identical. This agrees with findings from previous studies (e.g. Maronga and Raasch (2013)), who reported similar entrainment fluxes for homogeneous and heterogeneous simulations in shear-driven boundary layers, while under convective conditions surface heterogeneities can have a significant impact on the mixed-layer top entrainment (van Heerwaarden and Guerau de Arellano 2008; Sühring et al. 2014). Furthermore, in contrast to the 23 August case, the moisture flux profiles for 1100, 1200 and 1300 CDT indicated a mixed regime, neither moistening nor drying, where the drying of the boundary layer by entrainment is well balanced by the surface latent heat flux.

The relative contribution from surface-induced dispersive fluxes to the total heat fluxes were zero for the homogeneous runs. The moisture fluxes in the heterogeneous runs had higher

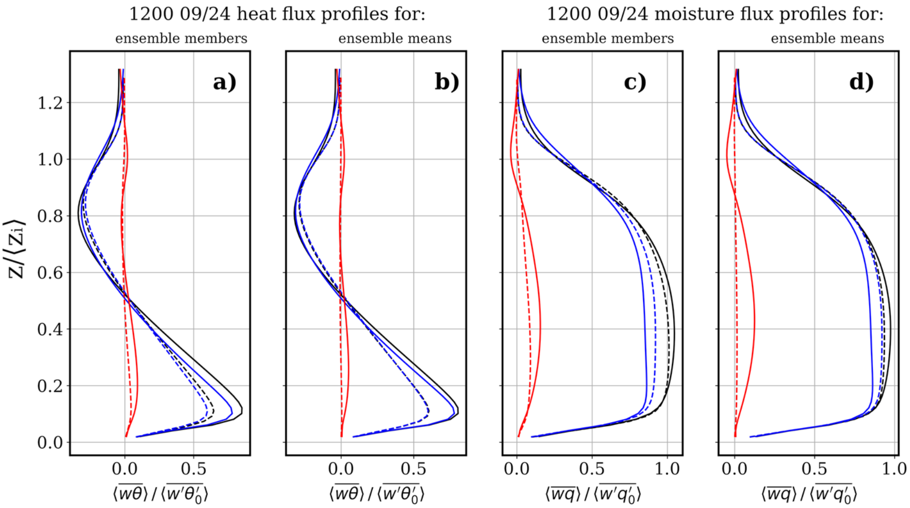

Fig. 8 Same as Fig. 6, but for the time period ending at 1200 CDT 24 September

surface-induced contributions than the heat fluxes. At 1200 (and 1300) CDT, the secondary circulations contributed 10–15% of the total near-surface ($0.1z_i$) heat and moisture vertical transport in the heterogeneous runs (seen in the solid red lines in Fig. 8a, c).

All of this suggests that surface heterogeneities can modify the spatial organisation of velocity and scalar fields in the near-neutral ABL and result in non-negligible covariances, even though the scalar fields are ’smeared’ by the higher near surface wind speeds and not exactly bound to surface horizontal gradients. This (also) indicates that the dispersive fluxes in the near neutral ABL are mostly due to turbulent organised structures.

3.4 Scale Analysis

In this section we investigate the scale composition of the simulated surface-induced atmospheric fields and their relationship to the length scales of the heterogeneous surface temperature and moisture fields. Our analysis of the heterogeneity induced persistent circulations during the 1100 CDT 23 August simulations and 1200 CDT 24 September simulations are presented here. The scale composition of the covariance between surface fluxes and surface-induced atmospheric fields are also discussed for the 23 August runs.

Simulation data were rotated to the mean ABL wind direction (calculated for the entire Child01 model), so that positive x direction corresponds to along-wind distance and positive y direction cross-wind distance. Since the flow organised as along-wind rolls, and these circulations and spatial organisations extend to the whole length of the study domain in the along-wind direction, Fourier spectral analysis only in the cross-wind direction is presented here. Their length scale composition in the along-wind direction within the study domain was composed of a long wavelength signal, of the order of the study domain length at every model height, and hence not studied in detail here.

1D Fourier spectra and cospectra were calculated at each model heights and for each cross-wind transect. The averaged spectral powers at each height were normalised by the total spectral power.

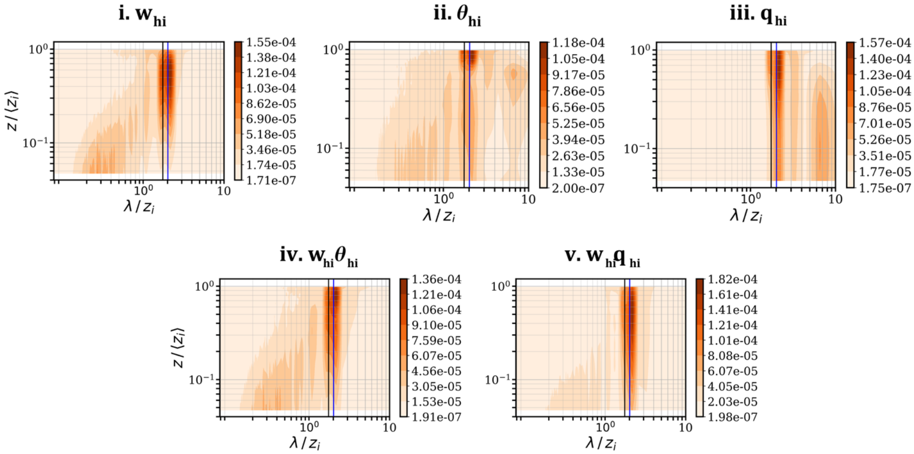

Fig. 9 Spectrograms of normalised cross-wind Fourier spectral densities of the surface heterogeneity induced **a** w, **b** θ, **c** q and cospectral densities of **d** w_{hi} and θ_{hi} and **e** w_{hi} and q_{hi} for the 23 August simulations at 1100. x-axis values are the wavelengths normalised by the domain mean z_i and y-axis is the vertical distance from the surface normalised by domain mean z_i. The solid vertical black line represents $L_{\theta y}$ and the solid vertical blue line represents L_{qy} from Fig. 3

3.4.1 Length Scales of Persistent Surface Heterogeneity Induced Fields

At 1100 CDT for 23 August simulations, the cross-wind surface temperature and moisture length scales ($L_{\theta y}$, L_{qy}) were of the order of $2\langle z_i\rangle$. The w_{hi}, θ_{hi} and q_{hi} spectra showed higher powers at spatial wavelengths corresponding to these cross-wind, surface length scales (Fig. 9a–c).

The w_{hi} spectra showed higher powers in wavelengths $\sim L_{qy}$ and $L_{\theta y}$ throughout the boundary layer height. Closer to the surface smaller than z_i scale w_{hi} eddies had also higher power. This could indicate localisation of near-surface turbulent eddies by surface heterogeneities that coalesce into the larger ABL scale rolls. The θ_{hi} and q_{hi} spectra were similar to the w_{hi} spectra with higher powers in wavelengths of the order of effective surface heterogeneity scales. The q_{hi} cross-wind spectra had a consistent maximum at L_{qy} throughout the ABL. There was a secondary maximum at higher powers too, extending from surface upwards. This could be due to entrainment effects, that can cause the near-surface q spatial field to have longer wavelength contributions (Couvreux et al. 2005), however a detailed analysis of links between surface-induced fields and entrainment flow is needed to establish a causal link.

Both the heterogeneity induced heat, and moisture flux cospectra showed higher cross-wind powers at surface length scales as well (Fig. 9d, e). The w_{hi} and θ_{hi} cospectra showed spectral power distribution more closely resembling the w_{hi} spectra. The w_{hi} and q_{hi} cospectra showed a consistent peak at surface length scales throughout the ABL, similar to both the w_{hi} and q_{hi} spectra. There was also a secondary maximum in the spectrograms of w_{hi} and $w_{hi}\theta_{hi}$ at wavelengths just greater than z_i. We calculated effective surface length scales as those length scales that contribute towards $2/3^{rds}$ of the simulated near-surface variance in temperature and moisture. In that sense, they correspond to 'cumulative' length scales, encompassing contributions from surface features that significantly impact atmospheric organisation. All of the diagnosed maxima occur at spatial scales greater than z_i, which could be approximated as the largest spatial scale of turbulent eddies, giving further confidence in our time-ensemble mean diagnosis of surface-induced organisations.

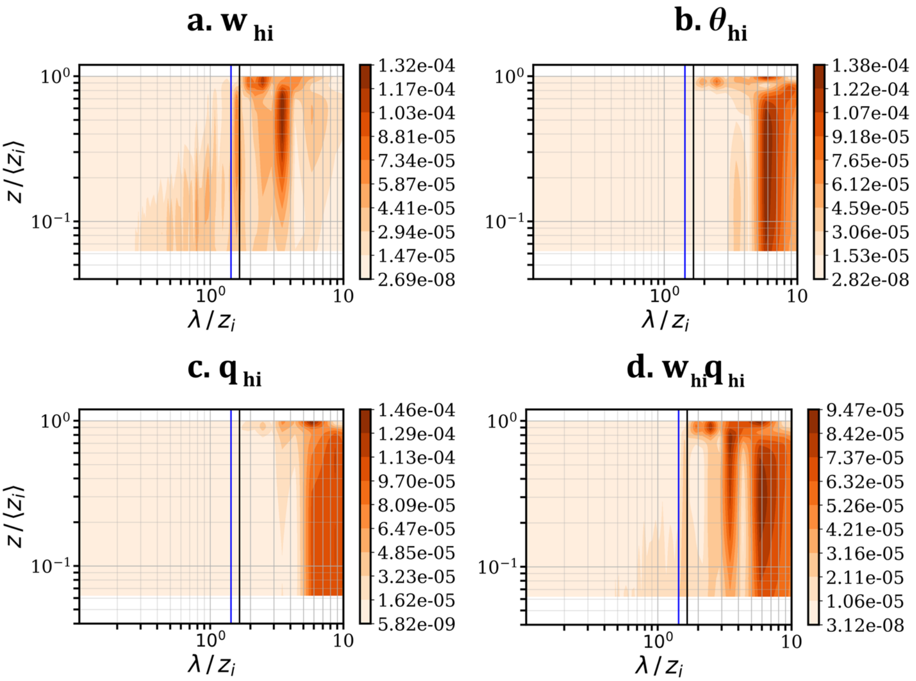

Fig. 10 Spectrograms of normalised cross-wind Fourier spectral densities of the surface heterogeneity induced **a** w, **b** θ, **c** q, and the cospectral density of **d** w_{hi} and q_{hi} for the 24 September simulations at 1200. x-axis values are the wavelengths normalised by the domain mean z_i and y-axis is the vertical distance from the surface normalised by domain mean z_i. The solid vertical black line represents $L_{\theta y}$ and the solid vertical blue line represents L_{qy} from Fig. 3

The cross-wind length scales of the time-ensemble mean atmospheric fields at 1200 CDT 24 September heterogeneous runs had maxima at larger scales than the surface length scales (Fig. 10). Spectrograms for w_{hi} showed higher power at spatial scales less than z_i near the surface. This could be due to the higher vertical wind-shear and stronger mechanical mixing near the surface in the forced convective boundary layer causing imprints of local, smaller scale surface roughness and thermal elements in the time-ensemble mean field, as seen in the $0.1z_i$ horizontal cross section (Fig. 5). There was a distinct maximum due to wavelengths that scaled as $3z_i$-$4z_i$ at model heights of $0.1z_i$ and higher.

The θ_{hi} and q_{hi} fields had spectral power at wavelengths greater than surface length scales and the boundary layer height throughout the ABL height, indicating that their spatial organisation, although modulated by the surface was not bound strictly to surface length scales. The cospectral density of w_{hi} and q_{hi} showed spectral peaks similar to the w_{hi} spectra and q_{hi} spectra. At heights near the boundary layer top there was a peak at $2.5z_i$, similar to the w_{hi} spectra, suggesting some indication of entrainment driven transport.

3.4.2 Surface Atmospheric Interactions

To explore the correlations between the diagnosed heterogeneity induced boundary layer structures and surface fluxes, we calculated spectrograms for the cospectra of surface fluxes ($w\theta_0$ and wq_0) with the heterogeneity induced atmospheric fields, w_{hi}, θ_{hi}, q_{hi} and the heterogeneity induced fluxes $w_{hi}\theta_{hi}$, $w_{hi}q_{hi}$ for the 1100 CDT 23 August simulations.

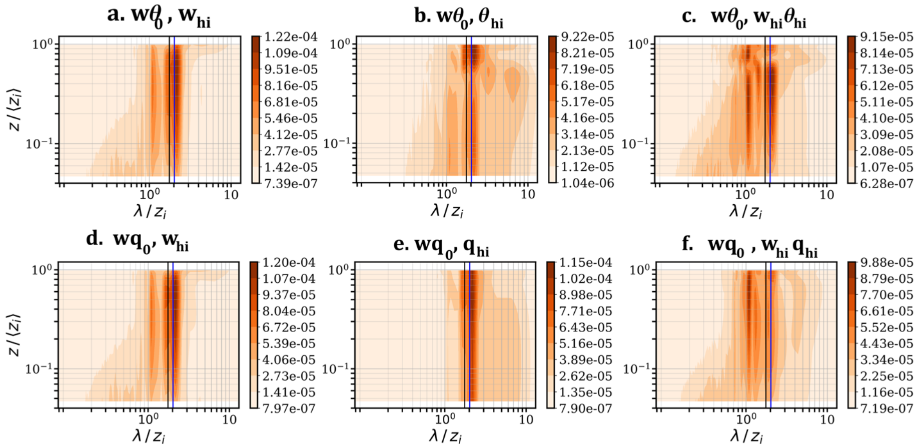

Fig. 11 Spectrograms of normalised cross-wind Fourier cospectral densities between surface heat ($w\theta_0$, in the 1^{st} row) and moisture(wq_0, in the 2^{nd} row) fluxes and the surface heterogeneity induced fields (a, d w_{hi}; b θ_{hi}; e q_{hi}) and fluxes(c $w_{hi}\theta_{hi}$; f $w_{hi}q_{hi}$). x-axis values are the wavelengths normalised by the domain mean z_i and y-axis is the vertical distance from the surface normalised by domain mean z_i. The solid vertical black line represents $L_{\theta y}$ and the solid vertical blue line represents L_{qy} from Fig. 3

At 1100 CDT, the surface heat and moisture flux cospectra with w_{hi} (Fig. 11a, d) look similar to the w_{hi} spectra (Fig. 9a). There is a distinct peak at the effective surface length scales, throughout the ABL height, indicating that the heterogeneity induced vertical wind and surface fluxes were correlated in the cross-wind direction at length scales ~ surface length scales. This resulted in the heterogeneity induced fluxes $w_{hi}\theta_{hi}$ and $w_{hi}q_{hi}$ with peak spectral power in the same surface length scales.

The cospectra of $w\theta_0$ with θ_{hi} showed a peak at the surface length scales, similar to the θ_{hi} spectra. Spectral maxima in the wq_0 q_{hi} cospectra were more consistent with height (Fig. 11e).

The cospectra of surface fluxes with heterogeneity induced fluxes showed higher spectral powers at a range of wavelengths. They suggest a superposition of the surface flux cospectra with w_{hi} and their respective heterogeneity induced scalar fields with the highest power capped at spatial scales ~ surface length scales. Figure 11 c, for the cospectra of surface heat flux with surface heterogeneity induced heat flux, higher contribution to the cospectra near the surface from smaller scale eddies like the cospectra of surface heat flux with w_{hi}. There were also higher powers at larger scales, ~ z_i^+ (the '+' sign denoting powers in wavelengths just greater than z_i) and $2z_i$ (of the order of surface length scales) consistently through most of the ABL height. The normalised cospectra of surface moisture flux was closer qualitatively to the cospectra of surface moisture flux with w_{hi}, with the distinct peak at wavelengths ~ z_i^+, suggesting that the impact of surface-moisture flux on the surface-induced moisture flux was mediated by the surface-induced vertical wind field.

4 Summary and Outlook

We performed diurnal LESs of the CHEESEHEAD19 field experiment days. The surface boundary conditions were informed by a coupled LSM representative of the heterogeneous CHEESEHEAD19 field experiment study domain. Non-stationary lateral and top boundary conditions were prescribed for the simulations using the HRRR model data to include a realistic diurnal evolution for the simulated ABLs. We used time-ensemble averaging to diagnose secondary circulations in the ABL induced by the land surface. We performed homogeneous control runs with the same lateral and top boundary conditions, but a homogeneous surface flux forcing. The domain-mean, above canopy H and LE from the heterogeneous runs were prescribed as the homogeneous surface flux forcing time series. In this manuscript, we focused on the simulated daytime data during the 23 August and 24 September simulations, when all of the ABL was fully resolved in our Child01 model.

4.1 On the Role of Effective Surface Length Scales

Our first research question was: How do the length scales of irregular, unstructured heterogeneities modulate the spatial organisation of secondary circulations in the heterogeneously heated ABL?

The ABL simulated for the 23 August IOP day of the CHEESEHEAD19 field experiment was free convective and buoyancy driven, with $-z_i/L \sim \mathcal{O}(10)$. In the weakly convective morning ABL ($-z_i/L \in [10,30]$), as the daytime boundary layer was developing, the cross-wind, surface length scales, normalised by z_i were greater than 1. With surface length scales greater than the boundary layer height, the effective cross-wind heterogeneity was not blended in the weakly convective boundary layer by near-surface turbulence. The w_{hi} fields diagnosed at 1100 CDT (representative of the morning ABL) for simulations with heterogeneous surface forcings had roll-like circulations, aligned roughly along-wind. The structures of the spatial fluctuation field were similar to the time-mean ABL organisation for 30-minute mean fields. Such roll-like spatial organisation was lacking in the homogeneously forced simulations, indicating that surface heterogeneities caused ABL roll-like organisation to become spatially localised. The same roll-like structure was seen in the diagnosed θ_{hi} and q_{hi} fields at 1100 CDT. Spectral analysis of the surface-induced atmospheric fields revealed maximum contribution from wavelengths that scaled as the effective surface length scales, consistently throughout the vertical extent of the ABL.

Later during the day, in our study domain, as the ABL grew and became fully developed from 1300–1600 CDT, the surface length scales became smaller than z_i. Even though the ABL was more free convective ($-z_i/L \in [48,60]$), with less near-surface mechanical mixing by atmospheric turbulence, the heterogeneous and homogeneous runs had similar spatial organisation for the velocity and scalar fields. The normalised spatial fluctuations from domain mean values for the time-ensemble mean fields were qualitatively similar for both test cases.

Our results are in accordance with prior idealised modelling studies, which indicated that the strength of surface-induced atmospheric fields depend on the relative magnitude of surface length scales and boundary layer height (Shen and Leclerc 1995; Raasch and Harbusch 2001; Patton et al. 2005; Sühring and Raasch 2013). However, our realistic simulations of the 24 September forced-convective ABL indicate that atmospheric static stability also plays an important role in modulating the spatial organisation of heterogeneity induced circulations. Moreover, it also affected the relative organisation of velocity and scalar fields, thereby modulating their covariances and ABL transport.

In the 23 August simulations, the heterogeneity induced secondary circulations started to transition from along-wind horizontal convective rolls in the morning boundary layer at 1100 CDT to quasi-localised cellular structures around 1300–1330 CDT when $-z_i/L \approx 40$. This value of ≈ 40 is higher than what has been reported in some of the previous observational and homogeneous simulation studies (Grossman (1982); Weckwerth et al. (1999); Salesky et al.

(2017); -$z_i/L \approx 15-25$). The delayed break down of roll-like structures in our heterogeneous simulations with respect to the prior reported threshold could be due to the memory in the diurnal evolution of surface heat fluxes and boundary layer winds. LeMone et al. (2010) reported observed roll-like organisation from tower measured values of -$z_i/L = 49$ and LES values of 41. The transition from horizontal rolls to cellular or disorganised local convection needs to be quantified by an objective metric for linear organisation, like the Roll factor proposed by Salesky et al. (2017) which is a two-point correlation metric calculated in cylindrical coordinates.

The near-neutral, wind shear driven ABL simulated for the 24 September test case, had smaller ABL heights than the free convective 23 August simulations, and the normalised effective surface heterogeneity scales remained greater than 1 for a larger part of the daytime simulations. There were distinct differences in the spatial organisation of atmospheric fields between the heterogeneous and homogeneous runs for these simulations as well, indicating signals of surface induced circulations. However, the spatial organisation of the velocity and scalar fields in the heterogeneous runs displayed larger length scales than the surface length scales.

The effective surface length scales for the 1100 CDT 23 August simulations and 1200 CDT 24 September simulations were approximately the same order of magnitude ($\sim 2z_i$). However, in the 24 September simulations, the surface length scales did not impose themselves on the ABL flow as strongly as the 1100 CDT 23 August simulations. Please note that nor were they inconsequential for the flow organisation like the afternoon 1400 CDT 23 August simulations.

To summarise, the stronger near-surface turbulent mechanical mixing in the wind-shear driven boundary layer smears out some effects of surface heterogeneity, however the larger effective surface length scales cause a non-negligible organisation of the ABL flow field.

4.2 Vertical Transport in the Horizontally Heterogeneous Boundary Layer

Our second research question was: How is the contribution from surface-induced secondary circulations to the area averaged mixed layer transport controlled by ABL static stability and surface length scales?

In the 23 August early morning simulations, when $L_{eff}/z_i > 1$, the spatially localised structures of w_{hi} were propagated to the simulated scalar fields of θ and q. Thus, there was a substantial contribution to the dispersive heat and moisture fluxes through surface-induced circulations. Later during the day, as the ABL grew and became fully developed, z_i became larger than the effective surface length scales. Even though the ABL was more free convective (-$z_i/L \in [30,60]$), since the relative surface length scales were smaller, the contributions from surface induced fluxes to area averaged transport were negligible. The dispersive fluxes over the study domain were caused mostly by turbulent organised structures. Here, the surface effects were blended by turbulent mixing in the boundary layer.

At 1100 CDT, the surface-induced dispersive flux contributions were $\sim 50\%$ of surface fluxes at $0.6z_i$. This result is in line with prior idealised studies Chen and Avissar (1994); Patton et al. (2005) who found that secondary circulations can contribute up to 50–80% of the total flux transport but in contrast to MR13 who reported lower values, 20% for heat and 39% for moisture.

In the wind-shear driven ABLs simulated for 24 September test case, L_{eff}/z_i was greater than 1 for most of the simulated daytime. Here, the surface-induced vertical velocity and scalar fields were not as tightly coupled as the weakly convective 1100 CDT 23 August runs. However, there was a non-negligible covariance between w_{hi} and θ_{hi},q_{hi}, resulting in a surface-induced dispersive flux, which was also higher than the values simulated for the afternoon free convective boundary layer for 23 August, when $L_{eff}/z_i < 1$.

4.3 Choice of Control Volume

We had to restrict our analysis within a $10 \times 10\,\text{km}^2$ subset of the Child01 model domain to remove edge effects that arose from nesting within the Parent domain. This removed analysis of circulations due to edge effects from the large lake to the north of Child01 in this manuscript. However, dispersive fluxes are a function of space. Hence, the choice of model domain, or measurement domain would determine the dispersive flux contribution within it. If one considers the entire Child01 model domain, the Turtle-Flambeau Flowage lake (black star in Fig. 1) imposes a length scale of $\sim 8\,\text{km}$ North-South and $3\,\text{km}$ West-East in the Child02 model domain). This creates a persistent surface horizontal gradient in surface fluxes throughout the daytime boundary layer evolution. 23 August simulations had north-easterly changing to easterly above-canopy winds. So, considering the North–South flux gradient imposed by the lake edge, for the whole Child01 domain L_{eff}/z_i would be greater than 1, assuming the domain mean z_i for Child01 model domain stays at a realistic value of about 2000 km.

So, unlike what we saw for the smaller $10 \times 10\,\text{km}^2$ subset during the late afternoon CBL, one can expect surface-induced standing circulations tied to the lake edges and dispersive flux transport caused due to these circulations. Such modulation of the atmospheric fields is visible in the 30-minute mean w,θ, and q, fields at $0.5z_i$ at 1400 CDT for 23 August (Online Resource 4: Fig. 16). The wind-shear driven 24 September simulations, had northerly above-canopy winds. The strong mean winds caused stronger advection of cold-moist air downstream from the lakes, unlike in the free convective 23 August simulations, where the heterogeneity effects were more localised. Moreover the θ_{hi} and q_{hi} fields in the 24 September simulations had larger cross-wind length scales than the w_{hi} fields, resulting in lower correlation and lower dispersive fluxes, even though the lake-induced θ_{hi} and q_{hi} fields have a longer fetch. We suppose this could be due to the weakened correlation between vertical velocity and scalar fluctuations in the wind-shear driven near-neutral ABL, where momentum fluxes dominate and near-surface turbulent vertical velocity fluctuations are primarily driven by horizontal velocity fluctuations (Mahrt 1991; Li and Bou-Zeid 2011).

The direction of the mean wind relative to horizontal gradients of surface properties can have a strong impact on the morphology of secondary circulations. Idealised LES studies have reported that span-wise surface heterogeneities can excite roll-like secondary circulations aligned roughly along the mean wind direction, while surface heterogeneities perpendicular to the mean flow can cause internal boundary layers (IBL) to develop and persist (Raasch and Harbusch 2001; Prabha et al. 2007; Fogarty and Bou-Zeid 2023). We find that the diagnosed surface-induced vertical velocity field follows a similar pattern (Online Resource 6: Fig. 18).

The lake edge perpendicular to the incoming wind developed an IBL like circulation, perpendicular to the mean flow at 1430 CDT 23 August. Likewise, the lake edge parallel to the mean flow developed a roll-like circulation whose axis aligned to the mean wind. The presence of the circulations clearly illustrates how dispersive fluxes change with changing control volume of choice. In this study we looked only at the cross-wind length scales and organisation to simplify our analysis and have a preliminary understanding of surface-induced ABL transport.

4.4 Perspectives on Past, Present and Future Work

Using data from the 30 m and 122 m levels of the US-PFa tall tower at the centre of the CHEESEHEAD19 domain, Xu et al. (2018) computed the 3D net surface atmosphere exchange over a control volume, including low frequency contributions from storage and vertical advection terms based on the Environmental Response Functions - Virtual Control Volume (ERF-VCV) approach (Metzger 2018). They computed the flux fields over a 10×10 km^2 domain, covering the core CHEESEHEAD19 study area. To include the low frequency contributions and project single tower measurements over the study domain, ERF-VCV relates morlet-wavelet calculated fluxes to relevant surface driver fields via footprint estimates by extracting relationships through boosted regression trees (Metzger et al. 2013; Xu et al. 2017).

The simulated, heterogeneity-induced circulation horizontal lengths scale as the effective surface heterogeneity length scales as well. In their sensitivity analysis with measurements at 122 m, Xu et al. (2018) reported that ensemble mean temporal standard deviation of heat fluxes decreased and stabilised at spatial transporting scale of 10–15 km. These findings indicate that over a heterogeneous domain, for the summer time convective boundary layer (with z_i $\sim$ 2 km) a bounding box $\sim$ 10 km would be sufficient to include this surface heterogeneity induced transport. Xu et al. (2018) also reported a 20% increase for the domain mean fluxes ($H + LE$) when volume correcting the 122 m fluxes for storage and vertical advection over the 10×10 km^2 domain averaged over the summertime months of July and August 2014. The simulated dispersive flux contribution in our runs at 120 m for 23 August was at 14% of total, close to values from the experimental scaling approaches. The slightly lower values in simulations could be because contributions from storage terms are not included in our study.

4.5 Conclusions

We hypothesised that over irregular, unstructured surface heterogeneities, one can define cross-wind surface length scales that impose themselves on the ABL flow and modulate the transport due to surface-induced circulations to the area averaged flux transport in the ABL via the dispersive fluxes they induce. Comparisons of the spatial fluctuation fields of time-ensemble means of the simulated atmospheric variables between heterogeneously and homogeneously forced simulations revealed that there were distinct differences between the two, mediated by the magnitudes of normalised effective surface length scales (L_{eff}/z_i) and the ABL static stability. The surface induced velocity and scalar fields in the heterogeneous runs resemble the spatial organisation of time-mean flow, unlike in the homogeneous case, indicating that the turbulent ABL spatial organisation is spatially localised by the irregular, heterogeneous surface.

We found stronger contributions from the dispersive fluxes during the free convective summer months, when the tower measured surface energy balance residuals were also higher (Butterworth et al. 2024). Note that the contribution from the dispersive fluxes would only explain a part of the measured residuals, with storage terms and flux divergence terms playing some part at individual tower locations. Nevertheless, in our simulations we find a substantial domain mean contribution from the dispersive fluxes and their heterogeneity induced components for the convective boundary layers. The simulated near-surface dispersive flux contribution for both the heat and moisture fluxes were 10–15% of the total daytime surface fluxes for the convective boundary layer (CBL) simulations. In the wind shear driven, near neutral ABL, the near-surface contribution of dispersive heat fluxes remained at 10–15% of total surface fluxes while the dispersive moisture flux contributions were lower than 5%. Our results support previous and ongoing work based on scale-aware up-scaling approaches over the heterogeneous forested study domain, that consider the low frequency contributions to storage and vertical advection terms. At the footprint scale of individual towers contributions from mesoscale circulations through dispersive fluxes would manifest in local advective terms as the horizontal branches of the secondary circulations would cause advective flux transport near surface. There would then be a balance between the contributions from dispersive fluxes and the advective components to the measured imbalance based on the control volume one chooses (Morrison et al. 2021). We plan to explore this question further in a future study based on the high resolution data from the Child02 (Sect. 2.1) model.

Our study supports ongoing efforts to parameterise the contributions from secondary circulations to tower measured surface energy imbalance using non-local scaling factors (De Roo et al. 2018; Mauder et al. 2021; Wanner et al. 2022a): z_i, $u_* \,/\, w_*$ and effective surface heterogeneity length scales. Wanner et al. (2024) presents a model for the dispersive sensible and latent heat fluxes accounting for thermal surface heterogeneity. They used simulated virtual tower data from the Child02 model to validate their approach and investigate the model performance in a realistic simulations.

This study underscores the role of effective surface heterogeneity length scales and ABL static stability through the relative role of wind shear vs buoyancy, in modulating surface-induced secondary circulations over irregular, unstructured heterogeneities. We present a simple framework to diagnose their contributions towards area averaged surface atmospheric transport, based on identifying cross-wind surface length scales from spatial maps of surface (or above canopy for vegetated surfaces) temperature and moisture fields. Our findings about the atmospheric coupling to surface heterogeneity scales can hence inform consistent assumptions for the impact of sub-grid heterogeneity in land surface schemes and ABL/convection schemes while representing the sub-grid coupling between land surface and atmospheric heterogeneities in weather and general circulation models.

Appendix 1: Ensemble Convergence

See Fig. 12.

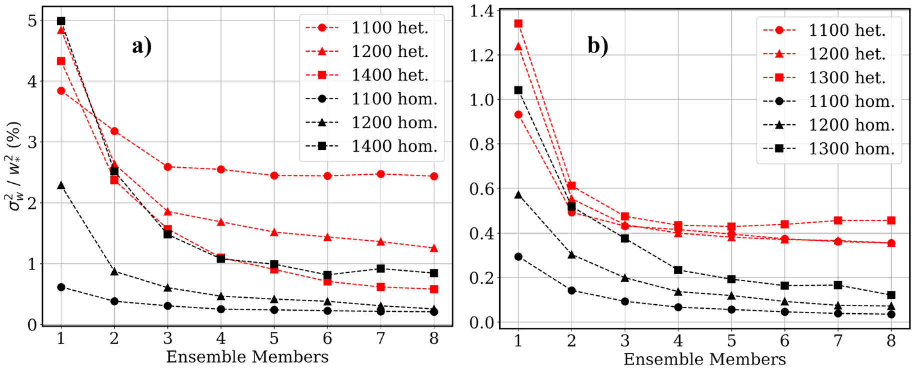

Fig. 12 ABL mean horizontal spatial variance of vertical wind for increasing number of ensemble members (N), at for 23 August (**a**) and 24 September (**b**). Red lines denote values for the heterogeneous simulations and black lines the homogeneous simulations. Time periods are indicated in the legends

Supplementary Information The online version contains supplementary material available at https://doi.org/10.1007/s10546-024-00893-7.

Acknowledgements This material is based in part upon work supported by the National Science Foundation through the CHEESEHEAD19 project (Grant AGS-1822420, AGS-2313772). The contribution of Luise Wanner was supported by Deutsche Forschungsgemeinschaft (DFG)Award #406980118 and the MICMoR Research School of KIT. For Sreenath Paleri additional funding was provided by NOAA/Office of Oceanic and Atmospheric Research under NOAA-University of Oklahoma Cooperative Agreement #NA21OAR4320204, U.S. Department of Commerce. We thank the developers of PALM at the Institute of Meteorology and Climatology of Leibniz University Hannover, Germany for the open source model and their technical support. We would like to acknowledge high-performance computing support from Cheyenne (doi:10.5065/D6RX99HX) and the Derecho system (doi:10.5065/qx9a-pg09) provided by the NSF National Center for Atmospheric Research (NCAR), sponsored by the National Science Foundation.

References

Albertson JD, Kustas WP, Scanlon TM (2001) Large-eddy simulation over heterogeneous terrain with remotely sensed land surface conditions. Water Resour Res 37(7):1939–1953

Anderson W, Barros JM, Christensen KT, Awasthi A (2015) Numerical and experimental study of mechanisms responsible for turbulent secondary flows in boundary layer flows over spanwise heterogeneous roughness. J Fluid Mech 768:316–347

Arakawa A, Lamb VR (1977) Computational design of the basic dynamical processes of the ucla general circulation model. General Circ Models Atmos 17(Supplement C):173–265

Atkinson B, Wu Zhang J (1996) Mesoscale shallow convection in the atmosphere. Rev Geophys 34(4):403–431

Avissar R, Schmidt T (1998) An evaluation of the scale at which ground-surface heat flux patchiness affects the convective boundary layer using large-eddy simulations. J Atmos Sci 55:24

Benjamin SG, Weygandt SS, Brown JM, Hu M, Alexander CR, Smirnova TG, Olson JB, James EP, Dowell DC, Grell GA, Lin H, Peckham SE, Smith TL, Moninger WR, Kenyon JS, Manikin GS (2016) A north American hourly assimilation and model forecast cycle: The rapid refresh. Mon Weather Rev 144(4):1669–1694

Betts AK, Ball JH, Beljaars AC, Miller MJ, Viterbo PA (1996) The land surface-atmosphere interaction: a review based on observational and global modeling perspectives. J Geophys Res: Atmos 101(D3):7209–7225

Blanford J, Bernhofer C, Gay L (1991) Energy flux mechanism over a pecan orchard oasis. In: Proceedings of the 20th agricultural forest meteorology conference

Blaylock BK, Horel JD, Liston ST (2017) Cloud archiving and data mining of high-resolution rapid refresh forecast model output. Comput Geosci 109:43–50

Bou-Zeid E, Anderson W, Katul GG, Mahrt L (2020) The persistent challenge of surface heterogeneity in boundary-layer meteorology: a review. Boundary-Layer Meteorol 177:227–245

Brunsell NA, Mechem DB, Anderson MC (2011) Surface heterogeneity impacts on boundary layer dynamics via energy balance partitioning. Atmos Chem Phys 11(7):3403–3416. https://doi.org/10.5194/acp-11-3403-2011

Butterworth BJ, Desai AR, Townsend PA, Petty GW, Andresen CG, Bertram TH, Kruger EL, Mineau JK, Olson ER, Paleri S, Pertzborn RA, Pettersen C, Stoy PC, Thom JE, Vermeuel MP, Wagner TJ, Wright DB, Zheng T, Metzger S, Schwartz MD, Iglinski TJ, Mauder M, Speidel J, Vogelmann H, Wanner L, Augustine TJ, Brown WOJ, Oncley SP, Buban M, Lee TR, Cleary P, Durden DJ, Florian CR, Lantz K, Riihimaki LD, Sedlar J, Meyers TP, Plummer DM, Guzman ER, Smith EN, Sühring M, Turner DD, Wang Z, White LD, Wilczak JM (2021) Connecting land-atmosphere interactions to surface heterogeneity in CHEESEHEAD19. Bull Am Meteor Soc 102(2):E421–E445. https://doi.org/10.1175/BAMS-D-19-0346.1

Butterworth BJ, Desai AR, Durden D, Kadum H, LaLuzerne D, Mauder M, Metzger S, Paleri S, Wanner L (2024) Characterizing energy balance closure over a heterogeneous ecosystem using multi-tower eddy covariance. Front Earth Sci 11(1251):138

Chen F, Avissar R (1994) The impact of land-surface wetness heterogeneity on mesoscale heat fluxes. J Appl Meteorol Climatol 33(11):1323–1340

Conzemius RJ, Fedorovich E (2006) Dynamics of sheared convective boundary layer entrainment. part i: Methodological background and large-eddy simulations. J Atmos Sci 63(4):1151–1178. https://doi.org/10.1175/JAS3691.1

Courault D, Drobinski P, Brunet Y, Lacarrere P, Talbot C (2007) Impact of surface heterogeneity on a buoyancy-driven convective boundary layer in light winds. Boundary-Layer Meteorol 124:383–403

Couvreux F, Guichard F, Redelsperger JL, Kiemle C, Masson V, Lafore JP, Flamant C (2005) Water-vapour variability within a convective boundary-layer assessed by large-eddy simulations and ihop_2002 observations. Q J R Meteorol Soc: J Atmos Sci Appl Meteorol Phys Oceanogr 131(611):2665–2693

De Roo F, Mauder M (2018) The influence of idealized surface heterogeneity on virtual turbulent flux measurements. Atmos Chem Phys 18(7):5059–5074. https://doi.org/10.5194/acp-18-5059-2018

de Roode SR, Duynkerke PG, Jonker HJ (2004) Large-eddy simulation: how large is large enough? J Atmos Sci 61(4):403–421

De Roo F, Zhang S, Huq S, Mauder M (2018) A semi-empirical model of the energy balance closure in the surface layer. PLOS ONE 13(12):e0209,022. https://doi.org/10.1371/journal.pone.0209022

Deardorff JW (1972) Numerical investigation of neutral and unstable planetary boundary layers. J Atmos Sci 29(1):91–115

Deardorff JW (1980) Stratocumulus-capped mixed layers derived from a three-dimensional model. Boundary-Layer Meteorol 18(4):495–527. https://doi.org/10.1007/BF00119502

Desai AR, Murphy BA, Wiesner S, Thom J, Butterworth BJ, Koupaei-Abyazani N, Muttaqin A, Paleri S, Talib A, Turner J, et al. (2022) Drivers of decadal carbon fluxes across temperate ecosystems. J Geophys Res: Biogeosci 127(12):e2022JG007,014

Drobinski P, Ra Brown, Flamant PH, Pelon J (1998) Evidence of organized large eddies by ground-based doppler lidar, sonic anemometer and sodar. Boundary-Layer Meteorol 88:343–361

Eder F, Schmidt M, Damian T, Träumner K, Mauder M (2015) Mesoscale eddies affect near-surface turbulent exchange: evidence from lidar and tower measurements. J Appl Meteorol Climatol 54(1):189–206. https://doi.org/10.1175/JAMC-D-14-0140.1

Etling D, Brown RA (1993) Roll vortices in the planetary boundary layer: a review. Boundary-Layer Meteorol 65(3):215–248. https://doi.org/10.1007/BF00705527

Fogarty J, Bou-Zeid E (2023) The atmospheric boundary layer above the marginal ice zone: scaling, surface fluxes, and secondary circulations. Boundary-Layer Meteorol 189(1):53–76

Garcia JR, Mellado JP (2014) The two-layer structure of the entrainment zone in the convective boundary layer. J Atmos Sci 71(6):1935–1955. https://doi.org/10.1175/JAS-D-13-0148.1

Grossman RL (1982) An analysis of vertical velocity spectra obtained in the bomex fair-weather, trade-wind boundary layer. Boundary-Layer Meteorol 23(3):323–357

Gryschka M, Gryanik V, Lüpkes C, Mostafa Z, Sühring M, Witha B, Raasch S (2023) Turbulent heat exchange over polar leads revisited: a large eddy simulation study. J Geophys Res: Atmos 128(12):e2022JD038,236

Hadfield M, Cotton W, Pielke R (1992) Large-eddy simulations of thermally forced circulations in the convective boundary layer. Part II: the effect of changes in wavelength and wind speed. Boundary-Layer Meteorol 58:307–327

Hadfield M, Cotton W, Pielke R (1991) Large-eddy simulations of thermally forced circulations in the convective boundary layer. part I: a small-scale circulation with zero wind. Boundary-Layer Meteorol 57(1):79–114

Harlow FH, Welch JE (1965) Numerical calculation of time-dependent viscous incompressible flow of fluid with free surface. Phys Fluids 8(12):2182–2189

Huang J, Lee X, Patton EG (2009) Dissimilarity of scalar transport in the convective boundary layer in inhomogeneous landscapes. Boundary-Layer Meteorol 130:327–345

Inagaki A, Letzel MO, Raasch S, Kanda M (2006) Impact of surface heterogeneity on energy imbalance: a study using LES. J Meteorol Soc Jpn 84(1):187–198. https://doi.org/10.2151/jmsj.84.187

Kadasch E, Sühring M, Gronemeier T, Raasch S (2021) Mesoscale nesting interface of the palm model system 6.0. Geosci Model Dev 14(9):5435–5465

Kanda M, Inagaki A, Letzel MO, Raasch S, Watanabe T (2004) LES study of the energy imbalance problem with eddy covariance fluxes. Boundary-Layer Meteorol 110(3):381–404. https://doi.org/10.1023/B:BOUN.0000007225.45548.7a

Kenny WT, Bohrer G, Morin TH, Vogel CS, Matheny AM, Desai AR (2017) A numerical case study of the implications of secondary circulations to the interpretation of eddy-covariance measurements over small lakes. Boundary-Layer Meteorol 165:311–332

Khanna S, Brasseur JG (1998) Three-dimensional buoyancy-and shear-induced local structure of the atmospheric boundary layer. J Atmos Sci 55(5):710–743

Kustas WP, Albertson JD (2003) Effects of surface temperature contrast on land-atmosphere exchange: a case study from monsoon 90. Water Resour Res 39(6)

LeMone MA, Chen F, Tewari M, Dudhia J, Geerts B, Miao Q, Coulter RL, Grossman RL (2010) Simulating the ihop_2002 fair-weather cbl with the wrf-arw-noah modeling system. part II: structures from a few kilometers to 100 km across. Mon Weather Rev 138(3):745–764

Lemone MA (1973) The structure and dynamics of horizontal roll vortices in the planetary boundary layer. J Atmos Sci 30(6):1077–1091

Lemone MA (1976) Modulation of turbulence energy by longitudinal rolls in an unstable planetary boundary layer. J Atmos Sci 33(7):1308–1320

Letzel MO, Raasch S (2003) Large eddy simulation of thermally induced oscillations in the convective boundary layer. J Atmos Sci 60(18):2328–2341

Li D, Bou-Zeid E (2011) Coherent structures and the dissimilarity of turbulent transport of momentum and scalars in the unstable atmospheric surface layer. Boundary-Layer Meteorol 140:243–262

Lin G, Wang Z, Chu Y, Ziegler CL, Hu XM, Xue M, Geerts B, Paleri S, Desai AR, Yang K, Deng M, DeGraw J (2024) Airborne measurements of scale-dependent latent heat flux impacted by water vapor and vertical velocity over heterogeneous land surfaces during the cheesehead19 campaign. J Geophys Res: Atmos 129(3):e2023JD039,586

Liu G, Sun J, Yin L (2011) Turbulence characteristics of the shear-free convective boundary layer driven by heterogeneous surface heating. Boundary-Layer Meteorol 140:57–71

Mahrt L (1991) Eddy asymmetry in the sheared heated boundary layer. J Atmos Sci 48(3):472–492

Mahrt L (2000) Surface heterogeneity and vertical structure of the boundary layer. Boundary-Layer Meteorol 96(1–2):33–62. https://doi.org/10.1023/A:1002482332477

Margairaz F, Pardyjak ER, Calaf M (2020) Surface thermal heterogeneities and the atmospheric boundary layer: the relevance of dispersive fluxes. Boundary-Layer Meteorol 175(3):369–395. https://doi.org/10.1007/s10546-020-00509-w

Maronga B, Raasch S (2013) Large-eddy simulations of surface heterogeneity effects on the convective boundary layer during the LITFASS-2003 experiment. Boundary-Layer Meteorol 146(1):17–44. https://doi.org/10.1007/s10546-012-9748-z

Maronga B, Banzhaf S, Burmeister C, Esch T, Forkel R, Fröhlich D, Fuka V, Gehrke KF, Geletič J, Giersch S, Gronemeier T, Groß G, Heldens W, Hellsten A, Hoffmann F, Inagaki A, Kadasch E, Kanani-Sühring F, Ketelsen K, Khan BA, Knigge C, Knoop H, Krč P, Kurppa M, Maamari H, Matzarakis A, Mauder M, Pallasch M, Pavlik D, Pfafferott J, Resler J, Rissmann S, Russo E, Salim M, Schrempf M, Schwenkel J, Seckmeyer G, Schubert S, Sühring M, von Tils R, Vollmer L, Ward S, Witha B, Wurps H, Zeidler J, Raasch S (2020) Overview of the palm model system 6.0. Geosci Model Dev 13(3):1335–1372

Mauder M, Ibrom A, Wanner L, De Roo F, Brugger P, Kiese R, Pilegaard K (2021) Options to correct local turbulent flux measurements for large-scale fluxes using an approach based on large-eddy simulation. Atmos Meas Tech 14(12):7835–7850. https://doi.org/10.5194/amt-14-7835-2021

Mazzaro LJ, Muñoz-Esparza D, Lundquist JK, Linn RR (2017) Nested mesoscale-to-les modeling of the atmospheric boundary layer in the presence of under-resolved convective structures. J Adv Model Earth Syst 9(4):1795–1810

Metzger S (2018) Surface-atmosphere exchange in a box: making the control volume a suitable representation for in-situ observations. Agric For Meteorol 255:68–80

Metzger S, Junkermann W, Mauder M, Butterbach-Bahl K, Trancón y Widemann B, Neidl F, Schäfer K, Wieneke S, Zheng X, Schmid HP, Foken T, (2013) Spatially explicit regionalization of airborne flux measurements using environmental response functions. Biogeosciences 10(4):2193–2217

Moeng CH, Wyngaard JC (1988) Spectral analysis of large-eddy simulations of the convective boundary layer. J Atmos Sci 45(23):3573–3587. https://doi.org/10.1175/1520-0469(1988)045<3573:SAOLES>2.0.CO;2

Moeng CH, Sullivan PP (1994) A comparison of shear-and buoyancy-driven planetary boundary layer flows. J Atmos Sci 51(7):999–1022

Morrison T, Calaf M, Higgins CW, Drake SA, Perelet A, Pardyjak E (2021) The impact of surface temperature heterogeneity on near-surface heat transport. Boundary-Layer Meteorol 180(2):247–272. https://doi.org/10.1007/s10546-021-00624-2

Paleri S, Desai AR, Metzger S, Durden D, Butterworth BJ, Mauder M, Kohnert K, Serafimovich A (2022) Space-scale resolved surface fluxes across a heterogeneous, mid-latitude forested landscape. J Geophys Res: Atmos, e2022JD037138

Paleri S, Wanner L, Sühring M, Desai AR, Matthias M, Metzger S (2023) Coupled large eddy simulations of land surface heterogeneity effects and diurnal evolution of late summer and early autumn atmospheric boundary layers during the cheesehead19 field campaign. Geosci Model Dev, under review

Patton EG, Sullivan PP, Moeng CH (2005) The influence of idealized heterogeneity on wet and dry planetary boundary layers coupled to the land surface. J Atmos Sci 62(7):2078–2097. https://doi.org/10.1175/JAS3465.1

Pielke RA, Avissar R, Raupach M, Dolman AJ, Zeng X, Denning AS (1998) Interactions between the atmosphere and terrestrial ecosystems: influence on weather and climate. Glob Change Biol 4(5):461–475

Prabha TV, Karipot A, Binford MW (2007) Characteristics of secondary circulations over an inhomogeneous surface simulated with large-eddy simulation. Boundary-Layer Meteorol 123:239–261

Raasch S, Harbusch G (2001) An analysis of secondary circulations and their effects caused by small-scale surface inhomogeneities using large-eddy simulation. Boundary-Layer Meteorol 101(1):31–59. https://doi.org/10.1023/A:1019297504109

Raupach MR, Shaw RH (1982) Averaging procedures for flow within vegetation canopies. Boundary-Layer Meteorol 22(1):79–90

Saiki EM, Moeng CH, Sullivan PP (2000) Large-eddy simulation of the stably stratified planetary boundary layer. Boundary-Layer Meteorol 95(1):1–30. https://doi.org/10.1023/A:1002428223156

Salesky S, Anderson W (2018) Buoyancy effects on large-scale motions in convective atmospheric boundary layers: implications for modulation of near-wall processes. J Fluid Mech 856:135–168

Salesky ST, Chamecki M, Bou-Zeid E (2017) On the nature of the transition between roll and cellular organization in the convective boundary layer. Boundary-Layer Meteorol 163(1):41–68. https://doi.org/10.1007/s10546-016-0220-3

Shen S, Leclerc MY (1995) How large must surface inhomogeneities be before they influence the convective boundary layer structure? A case study. Q J R Meteorol Soc 121(526):1209–1228

Steinfeld G, Letzel MO, Raasch S, Kanda M, Inagaki A (2007) Spatial representativeness of single tower measurements and the imbalance problem with eddy-covariance fluxes: results of a large-eddy simulation study. Boundary-Layer Meteorol 123(1):77–98. https://doi.org/10.1007/s10546-006-9133-x

Sühring M, Raasch S (2013) Heterogeneity-induced heat-flux patterns in the convective boundary layer: can they be detected from observations and is there a blending height?-A large-eddy simulation study for the LITFASS-2003 experiment. Boundary-Layer Meteorol 148(2):309–331. https://doi.org/10.1007/s10546-013-9822-1

Sühring M, Maronga B, Herbort F, Raasch S (2014) On the effect of surface heat-flux heterogeneities on the mixed-layer-top entrainment. Boundary-Layer Meteorol 151(3):531–556. https://doi.org/10.1007/s10546-014-9913-7

Sullivan PP, Moeng CH, Stevens B, Lenschow DH, Mayor SD (1998) Structure of the entrainment zone capping the convective atmospheric boundary layer. J Atmos Sci 55(19):3042–3064

Träumner K, Damian T, Stawiarski C, Wieser A (2015) Turbulent structures and coherence in the atmospheric surface layer. Boundary-Layer Meteorol 154:1–25

van Heerwaarden CC, Guerau de Arellano JV (2008) Relative humidity as an indicator for cloud formation over heterogeneous land surfaces. J Atmos Sci 65(10):3263–3277

van Heerwaarden CC, Mellado JP, De Lozar A (2014) Scaling laws for the heterogeneously heated free convective boundary layer. J Atmos Sci 71(11):3975–4000. https://doi.org/10.1175/JAS-D-13-0383.1

Wanner L, De Roo F, Sühring M, Mauder M (2022) How does the choice of the lower boundary conditions in large-eddy simulations affect the development of dispersive fluxes near the surface? Boundary-Layer Meteorol 182(1):1–27

Wanner L, Jung M, Paleri S, Butterworth BJ, Desai AR, Sühring M, Mauder M (2024) Towards energy-balance closure with a model of dispersive heat fluxes. Boundary-Layer Meteorol 190(5):25

Wanner L, Calaf M, Mauder M (2022a) Incorporating the effect of heterogeneous surface heating into a semi-empirical model of the surface energy balance closure. PloS one 17(6):e0268,097

Weckwerth TM, Wilson JW, Wakimoto RM, Crook NA (1997) Horizontal convective rolls: determining the environmental conditions supporting their existence and characteristics. Mon Weather Rev 125(4):505–526

Weckwerth TM, Horst TW, Wilson JW (1999) An observational study of the evolution of horizontal convective rolls. Mon Weather Rev 127(9):2160–2179

Wicker LJ, Skamarock WC (2002) Time-splitting methods for elastic models using forward time schemes. Mon Weather Rev 130(8):2088–2097

Williamson JH (1980) Low-storage Runge–Kutta schemes. J Comput Phys 35(1):48–56

Wilson NR, Shaw RH (1977) A higher order closure model for canopy flow. J Appl Meteorol 1962–1982:1197–1205

Xie ZT, Castro IP (2008) Efficient generation of inflow conditions for large-eddy simulation of street-scale flows. Flow Turbul Combust 81(3):449–470

Xu K, Metzger S, Desai AR (2017) Upscaling tower-observed turbulent exchange at fine spatio-temporal resolution using environmental response functions. Agric For Meteorol 232:10–22

Xu K, Metzger S, Desai AR (2018) Surface-atmosphere exchange in a box: Space-time resolved storage and net vertical fluxes from tower-based eddy covariance. Agric For Meteorol 255:81–91

Zhou Y, Sühring M, Li X (2023) Evaluation of energy balance closure adjustment and imbalance prediction methods in the convective boundary layer-a large eddy simulation study. Agric For Meteorol 333(109):382